



Tsung-Hui Huang · Chia-Lien Chao

A stabilized one-point integrated mixed formulation for finite element and meshfree methods in modeling nearly incompressible materials

Received: 28 August 2021 / Revised: 13 November 2021 / Accepted: 3 December 2021 / Published online: 5 March 2022
© The Author(s), under exclusive licence to Springer-Verlag GmbH Austria, part of Springer Nature 2022

Abstract This study develops a stabilized Galerkin mixed formulation within a one-point integrated framework to model nearly incompressible materials. The variational multiscale formulation addresses the hourglass modes and Ladyzhenskaya–Babuska–Brezzi (LBB) instability in conventional Galerkin mixed formulation. The multiscale decomposition of the variational equation results in a residual-based stabilized Galerkin framework. The derived fine-scaled terms act as a stabilization that alleviates hourglass instability and pressure oscillations. The strain smoothing method is employed in coarse-scale terms to satisfy the integration constraint. A smoothed divergence is applied to the fine-scale terms to relax using a higher-order basis function. The proposed method is applied to the reproducing kernel particle method and the smoothed finite element method to demonstrate its efficacy in general meshfree and mesh-based methods. The effectiveness of the formulation is verified by solving a series of elasticity problems under the incompressible limit. The proposed method outperforms the other two classical stabilization approaches, which are also derived in this study.

1 Introduction

Robust modeling of incompressible media is a challenging task within the conventional displacement-based Galerkin paradigm, as over-constrained displacements, known as volumetric locking, are often encountered at the incompressibility limit of the material. Techniques such as the incompatible modes element [1] or enhanced/assumed strain method [2, 3] are used to alleviate locking. They involve enhancing the displacement approximation spaces. In addition, techniques such as selective reduced integration [4], B-bar [4] or F-bar [5, 6], and the pressure projection method [7–9] are popular within finite element method (FEM) and meshfree method. Although these methods have effectively addressed the locking issue, they have not yet been extended to truly incompressible media. In addition, the solution accuracy usually degenerates under the compressible regime.

Mixed formulation [10] is an alternative way to alleviate locking while retaining solution accuracy under different compressibility. By decoupling the volumetric stress from the displacement-based framework, a displacement–pressure Galerkin formulation is constructed. The pressure acts as the Lagrange multiplier to impose the volumetric constraint (incompressibility constraint). However, even though the mixed formulation is locking-free, it is well-known that such an approach suffers from the inherited Ladyzhenskaya–Babuska–Brezzi (LBB) instability [11, 12], where the pressure field becomes oscillatory under a careless selection of function spaces. In addition to the LBB instability, the quadrature rule also plays an essential role in the Galerkin mixed formulation. Conventionally, the Gauss quadrature is cumbersome and inaccurate [13, 14] for meshfree methods as well as meshfree-like mesh-based approach including smoothed FEM (S-FEM) [15], which will be elaborated later. It is also not suitable for large deformation problems [16, 17]. Consequently, nodal or reduced

one-point integration methods are preferable as they reduce the number of stress evaluation points and can be inherently applied to large deformations. Hence, the investigation and development of a robust one-point integration scheme for the Galerkin mixed formulation lie within the scope of this study. Here, we will use the terminology “one-point integration method” to represent nodal integration and generally reduced integration schemes in meshfree and mesh-based formulation [18].

The application of the mixed formulations for FEM and meshfree methods has been an area of active research for many years in the field of elasticity [19–21], inelasticity [22–25], and plasticity [26–29]. Malkus and Hughes [4, 30] proved that the mixed formulation is equivalent to a displacement-based formulation with a selective reduced integration. Chen et al. [31] and Kadapa et al. [32] proposed a perturbed Lagrangian approach for mixed finite element formulation and mixed isogeometric analysis (IGA [33]), respectively. In this approach, the perturbed Lagrange multiplier relaxes the incompressibility constraint and yields an accurate solution. However, the accuracy deteriorates for problems experiencing significant tension in the compressible regime. In addition, a penalty function is needed for the perturbed Lagrange multiplier method. Schroder et al. [34] proposed a novel consistent mixed formulation independent of the penalty parameters by generalizing the classical perturbed Lagrangian approach with different penalty functions in the incompressibility limit. However, such an approach is difficult to apply to the compressible case. To obtain a consistent solution under both compressible and incompressible regimes, variational multiscale formulation [35] (VMS) can be adopted, where the term “multiscale” is viewed as the computational scales in the solution to the Galerkin formulation. It was shown in earlier works by Hughes and Franca [36], Hughes et al. [37], and Franca et al. [38] that the VMS method for Stoke’s problem leads to a Galerkin least-squares term with a tunable parameter that stabilizes spurious node-to-node pressure oscillations. Here this early version was termed the Hughes variational multiscale (HVM) formulation. In the years that followed, different variants of HVM were proposed. Masud et al. [19, 22] employed the concept of HVM for elasticity and inelasticity, where the fine-scale variables are approximated with the bubble enrichment function such that the formulation is parameter-free. However, this approach is computationally inefficient due to additional degrees of freedom (DOFs) caused by the enrichment. In addition, the construction of the bubble function is complicated for meshfree methods [39]. Chiumenti et al. [29, 40, 41] tackled the mixed formulation by using the orthogonal subscale method, which is a variant of VMS introduced by Hughes et al. [37] and Codina [42]. This approach also required additional DOFs to be solved for the progress projection variables. Recently, Scovazzi et al. [24, 43] developed the dynamic version of HVM, called D-VMS, for dynamically incompressible inelastic materials. Such approaches enhance the robustness of HVM in dynamic problems. Although HVM and related works have achieved huge success for incompressible media and nonlinear mechanics, all these approaches focused on Gauss integration in the Galerkin framework instead of one-point integration techniques. This is inconvenient and inaccurate for meshfree approaches. Furthermore, higher-order gradients in the HVM formulation limit the employment of conventional FEM. These issues shall be investigated and addressed later.

Numerical quadrature plays an important role in the variational framework of meshfree and mesh-based methods. It is still considered the main bottleneck in many computational frameworks. Extensive development of one-point integration in recent years is explained in [16]. Simple one-point integration such as direct nodal integration (DNI) or reduced integration in FEM has been proven to be unstable due to rank deficiency. To address this issue, Chen et al. [44, 45] developed the well-known stabilization conforming nodal integration (SCNI) method by introducing a smoothed strain in satisfying the integration constraint in the Galerkin framework and successfully alleviated the rank deficiency. SCNI has been successfully applied to various solid mechanics problems for meshfree methods [16, 44, 45], including incompressible and nearly incompressible materials [14, 46, 47]. The idea of strain smoothing in SCNI was introduced to FEM by Liu et al. [48, 49], resulting in a class of S-FEMs and different methods of constructing the smoothing domains, such as the node-based S-FEM (NS-FEM) [50], cell-based S-FEM (CS-FEM) [51], edge-based S-FEM (ES-FEM) [52], and many other variants (see [17] for more details). They were also successfully applied to many solid mechanics problems [17, 53, 54] and incompressible materials [55–57]. Although it is successful in real-world applications, one-point integration with simple strain smoothing displays hourglass modes for both meshfree methods [58] and S-FEM [15, 59]. It may also suffer from temporal instability, as expressed in [17, 60]. As a result, enhancement on SCNI has been developed. A straightforward approach is to introduce additional strain smoothing on subdivided quadrature cells. This approach is called modified stabilized conforming nodal integration (MSCNI) in meshfree methods [21, 61, 62]. The subdomain smoothing approach was also adopted in S-FEM [15, 59]. However, the formulation is computationally expensive owing to extensive subdomain division. In addition, the formulation depends on a tunable parameter [62] or the optimal number of smoothing cells (e.g., in CS-FEM [48], four smoothing cells for Q4 element gave optimal accuracy). Unlike the subdomain

smoothing approach, the gradient stabilization method was developed in the meshfree method by Hillman and Chen [63] and was called naturally stabilized nodal integration (NSNI). A similar approach, namely strain gradient stabilization (SGS), was developed by Wu et al. [64]. In this approach, the stabilization was introduced via higher gradient strain terms in the Galerkin formulation and is nodally integrated without any subdomain divisions. Therefore, this approach still lies within the one-point integration class and is more efficient than MSCNI-type stabilization [26, 65]. NSNI was also recently introduced to the mixed geo-mechanical formulation [26]. For S-FEM, this gradient type of approach has also been introduced by Yang et al. [66], Chen et al. [67], and Feng et al. [68]. In these methods, the higher-order derivatives caused by gradient expansion are computed using a smoothing approach. Recently, Moutsanidis et al. [18] generalized the gradient-type approach for one-point integration for FEM, IGA, and immersed methods on incompressible materials, where the gradient correction is applied only to the deviatoric part of the internal energy. Progress has also been made for stabilization methods in one-point integration. Research on proper integration techniques for mixed formulations is rare and therefore deserves investigation.

In this study, we revisit the variational multiscale stabilization method and HVM and develop a stabilized Galerkin mixed formulation within a one-point integration technique. The method employs variational multiscale formalism [35] to decouple the weak form into coarse-scale and fine-scale problems, and multiscale analysis leads to residual-based stabilization within the Galerkin mixed formulation. The one-point integration with strain and the divergence smoothing method [69, 70] are employed to retain the higher-order terms in the formulation and satisfy the integration constraint in the Galerkin equation. The method was applied to reproducing kernel particle method (RKPM) [71] and CS-FEM in linear elasticity. We also extend the classical MSCNI and NSNI schemes in displacement-based formulation to the mixed formulation and then investigate their performance with the proposed VMS method. The proposed method alleviates the pressure oscillation and hourglass instability in the one-point integrated mixed formulation and still retains the locking-free property.

This paper is organized as follows. In Sect. 2, a brief review of the basic mixed formulation in elasticity and the strain smoothing technique in nodal integration is introduced. In Sect. 3, classical nodal stabilization techniques for mixed formulation are derived and discussed. In Sect. 4, the derivation for the variational multiscale method for the mixed formulation is provided, and a smoothed divergence operator is introduced. Benchmark problems are presented in Sect. 5 to investigate the performance of the proposed methods. Finally, conclusions are presented in Sect. 6.

2 Basic equations

2.1 Mixed formulation for linear elasticity

For a boundary value problem (BVP) of linear elasticity in a close domain $\bar{\Omega} = \Omega \cup \partial\Omega$, the strong form of the problem reads

$$\sigma_{ij,j} + b = 0 \quad \text{in } \Omega, \quad (1)$$

$$\sigma_{ij}n_j - t_i = 0 \quad \text{on } \partial\Omega_N, \quad (2)$$

$$u_i - g_i = 0 \quad \text{on } \partial\Omega_D \quad (3)$$

where b is the body load, σ_{ij} is the Cauchy stress tensor, n_i is the out-boundary normal, t_i and g_i are prescribed traction and essential boundary conditions on Neumann boundary $\partial\Omega_N$ and Dirichlet boundary $\partial\Omega_D$. The domain Ω admits the decomposition $\partial\Omega_D \cup \partial\Omega_N = \partial\Omega$ and $\partial\Omega_D \cap \partial\Omega_N = \emptyset$. The infinitesimal strain tensor is defined as

$$\varepsilon_{ij} = \frac{1}{2}(u_{i,j} + u_{j,i}). \quad (4)$$

In the case of linear isotropic elasticity, the Cauchy stress tensor σ_{ij} and strain tensor ε_{ij} have the following constitutive model:

$$\sigma_{ij} = 2\mu\varepsilon_{ij} + \lambda\varepsilon_{kk}\delta_{ij} \quad (5)$$

where μ and λ are the shear modulus and first Lamé parameter that can be computed from Young's modulus E and Poisson's ratio ν . When the material approaches the incompressibility limit, the Poisson's ratio $\nu \rightarrow 0.5$. In the mixed formulation, the hydrostatic pressure p is defined as

$$p = \lambda \varepsilon_{ii} = \lambda u_{i,i}, \quad (6)$$

and the weak form of the mixed formulation is required to find $(u_i, p) \in \mathcal{S}^u \times \mathcal{S}^p$ such that $\forall (\delta u_i, \delta p) \in \mathcal{V}^u \times \mathcal{V}^p$:

$$2\mu \int_{\Omega} \varepsilon_{ij}(\delta \mathbf{u}) \varepsilon_{ij}(\mathbf{u}) d\Omega + \int_{\Omega} \delta u_{i,i} p d\Omega = \int_{\Omega} \delta u_i b_i d\Omega + \int_{\partial\Omega_N} \delta u_i t_i d\Gamma, \quad (7)$$

$$\int_{\Omega} \delta p \left(u_{i,i} - \frac{p}{\lambda} \right) d\Omega = 0 \quad (8)$$

where \mathcal{S}^u , \mathcal{S}^p , \mathcal{V}^u , and \mathcal{V}^p are kinematically admissible function spaces for trial functions u_i , p , and test functions δu_i and δp , respectively. The function spaces are defined as follows:

$$\begin{aligned} \mathcal{S}^u &\equiv \{u_i | u_i \in H^1(\Omega), u_i = g_i \text{ on } \partial\Omega_D\}, \\ \mathcal{S}^p &\equiv \{p | p \in L_2(\Omega)\}, \\ \mathcal{V}^u &\equiv \{u_i | u_i \in H^1(\Omega), u_i = 0 \text{ on } \partial\Omega_D\}, \\ \mathcal{V}^p &\equiv \{p | p \in L_2(\Omega)\}. \end{aligned} \quad (9)$$

Next, the Galerkin equation of the weak form (7) and (8) reads as follows: find $(u_i^h, p^h) \in \mathcal{S}^{u^h} \times \mathcal{S}^{p^h}$ such that $\forall (\delta u_i^h, \delta p^h) \in \mathcal{V}^{u^h} \times \mathcal{V}^{p^h}$:

$$2\mu \int_{\Omega} \delta \varepsilon_{ij}^h \varepsilon_{ij}^h d\Omega + \int_{\Omega} \delta \varepsilon_{ii}^h p^h d\Omega = \int_{\Omega} \delta u_i^h b_i d\Omega + \int_{\partial\Omega_N} \delta u_i^h t_i d\Gamma, \quad (10)$$

$$\int_{\Omega} \delta p^h \left(\varepsilon_{ii}^h - \frac{p^h}{\lambda} \right) d\Omega = 0 \quad (11)$$

where $\mathcal{S}^{\alpha^h} \subset \mathcal{S}^{\alpha}$ and $\mathcal{V}^{\alpha^h} \subset \mathcal{V}^{\alpha}$ for $\alpha = u, p$. Here, the notation $\varepsilon_{ij}^h = \varepsilon_{ij}(\mathbf{u}^h)$ and $\delta \varepsilon_{ij}^h = \varepsilon_{ij}(\delta \mathbf{u}^h)$ is employed. In this study, the finite element (FE) approximation and the meshfree reproducing kernel (RK) approximation are used. An equal order approximation is adopted here such that the displacements and pressure are approximated via the same sets of shape function as follows:

$$u_i(\mathbf{x}) \approx u_i^h(\mathbf{x}) = \sum_{I \in G_{\mathbf{x}}} \Psi_I(\mathbf{x}) u_{Ii}, \quad (12)$$

$$p(\mathbf{x}) \approx p^h(\mathbf{x}) = \sum_{I \in G_{\mathbf{x}}} \Psi_I(\mathbf{x}) p_I \quad (13)$$

where \mathbf{x} represents the spatial coordinates, Ψ_I is the I -th nodal shape function for displacement and pressure, respectively. u_{Ii} and p_I are nodal coefficients for displacements and pressure, respectively. $G_{\mathbf{x}} = \{I | \Phi_a(\mathbf{x} - \mathbf{x}_I) \neq 0\}$ is the support for a given evaluation point \mathbf{x} . The construction of the RK shape function can be found in the "Appendix".

Then, by introducing the approximation shown in Eqs. (12) and (13) while invoking the arbitrariness of the test functions, the unknown displacements and pressure coefficients can be determined by solving the following matrix equation:

$$\begin{bmatrix} \mathbf{K}^{uu} & \mathbf{K}^{up} \\ \mathbf{K}^{pu} & \mathbf{K}^{pp} \end{bmatrix} \begin{bmatrix} \mathbf{u} \\ \mathbf{p} \end{bmatrix} = \begin{bmatrix} \mathbf{F}^u \\ 0 \end{bmatrix} \quad (14)$$

where the matrices and vectors in Eq. (14) are expressed as follows:

$$\mathbf{K}_{IJ}^{uu} = 2\mu \int_{\Omega} \mathbf{B}_I^T(\mathbf{x}) \mathbf{B}_J(\mathbf{x}) d\Omega, \quad (15)$$

$$\mathbf{K}_{IJ}^{up} = \mathbf{K}_{IJ}^{upT} = \int_{\Omega} \mathbf{B}_I^T(\mathbf{x}) \mathbf{1} \Psi_J(\mathbf{x}) d\Omega, \quad (16)$$

$$K_{IJ}^{pp} = -\frac{1}{\lambda} \int_{\Omega} \Psi_I(\mathbf{x}) \Psi_J(\mathbf{x}) d\Omega, \quad (17)$$

$$\mathbf{F}_I^u = \int_{\Omega} \mathbf{N}_I^T(\mathbf{x}) \mathbf{b}(\mathbf{x}) d\Omega + \int_{\partial\Omega_N} \mathbf{N}_I^T(\mathbf{x}) \mathbf{t}(\mathbf{x}) d\Gamma \quad (18)$$

with \mathbf{B}_I , \mathbf{N}_I , and $\mathbf{1}$ defined, respectively, as

$$\mathbf{B}_I = \begin{bmatrix} \Psi_{I,1} & 0 \\ 0 & \Psi_{I,2} \\ \Psi_{I,2} & \Psi_{I,1} \end{bmatrix}, \quad (19)$$

$$\mathbf{N}_I = \begin{bmatrix} \Psi_I & 0 \\ 0 & \Psi_I \end{bmatrix}, \quad (20)$$

$$\mathbf{1} = [1 \ 1 \ 0]^T. \quad (21)$$

To solve Eq. (14), a stable and accurate quadrature rule is required, which is introduced in the next Section.

2.2 Strain smoothing in one-point integration for mixed formulation

As discussed in the Introduction, Gauss integration is not suitable for a meshfree approach, and direct one-point integration for the Galerkin equation will result in spurious zero-energy modes. Such instability can be removed by the strain smoothing technique analogous to SCNI in [44], where strain smoothing within the meshfree nodal integration preserves the linear exactness in the Galerkin formulation and therefore precludes instability in pure one-point integration.

In SCNI, the smoothed strain is interpreted as follows:

$$\tilde{\varepsilon}_{ij}^h = \frac{1}{V_L} \int_{\Omega_L} \varepsilon_{ij}^h d\Omega = \frac{1}{2V_L} \int_{\partial\Omega_L} u_i^h n_j + u_j^h n_i d\Gamma \quad (22)$$

where Ω_L is the quadrature cell domain, $V_L = \text{meas}(\Omega_L)$ is the volume of the cell (or area for two-dimensional case), and n_i is the cell boundary outward normal as shown in Fig. 1. In the CS-FEM [51] approach, the element serves as the quadrature cell as shown in Fig. 1a. For meshfree methods such as RKPM, such quadrature cells can be constructed via a Voronoi tessellation as shown in Fig. 1b.

Then, by employing the strain smoothing method with one-point integration, the stiffness matrices in Eqs. (15)–(18) can be computed as follows:

$$\mathbf{K}_{IJ}^{uu} \approx \tilde{\mathbf{K}}_{IJ}^{uu} = 2\mu \sum_{L \in S} \tilde{\mathbf{B}}_I^T(\mathbf{x}_L) \tilde{\mathbf{B}}_J(\mathbf{x}_L) W_L, \quad (23)$$

$$\mathbf{K}_{IJ}^{up} \approx \tilde{\mathbf{K}}_{IJ}^{up} = \tilde{\mathbf{K}}_{IJ}^{upT} = \sum_{L \in S} \tilde{\mathbf{B}}_I^T(\mathbf{x}_L) \mathbf{1} \Psi_J(\mathbf{x}_L) W_L, \quad (24)$$

$$K_{IJ}^{pp} \approx \sum_{L \in S} \Psi_I^T(\mathbf{x}_L) \Psi_J(\mathbf{x}_L) W_L, \quad (25)$$

$$\mathbf{F}_I^u \approx \sum_{L \in S} \Psi_I^T(\mathbf{x}_L) \mathbf{b}(\mathbf{x}_L) W_L + \sum_{L \in S_N} \Psi_I^T(\mathbf{x}_L) \mathbf{t}(\mathbf{x}_L) W_L \quad (26)$$

where S and S_N are, respectively, the node sets containing all quadrature points in the domain and on the Neumann boundary, and \mathbf{x}_L and W_L are the quadrature point and associated quadrature weight, respectively. The quadrature points defined for CS-FEM and RKPM are also expressed in Fig. 1. $\tilde{\mathbf{B}}_I$ is the smoothed strain gradient matrix, and for the two-dimensional case, it can be expressed as

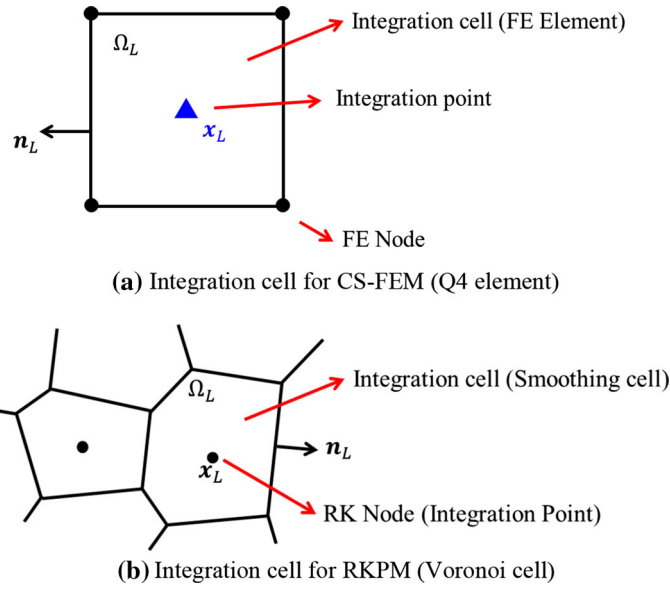


Fig. 1 Two-dimensional example of quadrature cell for **a** CS-FEM and **b** meshfree RKPM

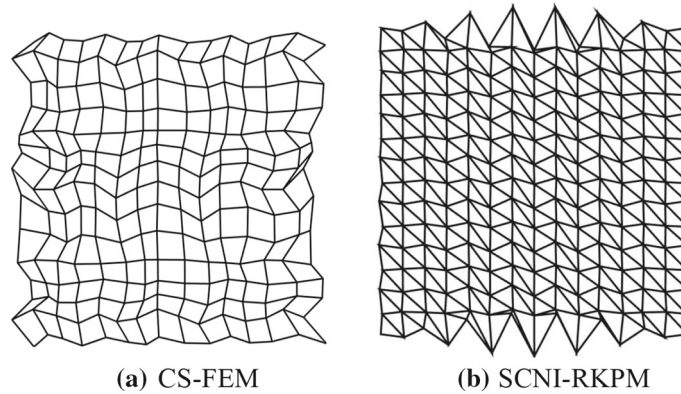


Fig. 2 Hourglass instability for pure strain smoothing in the one-point integration method for mixed formulation. The meshfree result is plotted using triangular discretization for visualization

$$\tilde{\mathbf{B}}_I(\mathbf{x}_L) = \begin{bmatrix} \tilde{\Psi}_{I,1}(\mathbf{x}_L) & 0 \\ 0 & \tilde{\Psi}_{I,2}(\mathbf{x}_L) \\ \tilde{\Psi}_{I,2}(\mathbf{x}_L) & \tilde{\Psi}_{I,1}(\mathbf{x}_L) \end{bmatrix} \tag{27}$$

where $\tilde{\Psi}_{I,i}(\mathbf{x}_L)$ is the smoothed gradient matrix computed as

$$\tilde{\Psi}_{I,i}(\mathbf{x}_L) = \frac{1}{V_L} \int_{\Omega_L} \Psi_{I,i}(\mathbf{x}) d\Omega = \frac{1}{V_L} \int_{\partial\Omega_L} \Psi_I(\mathbf{x}) n_i(\mathbf{x}) d\Gamma \tag{28}$$

and a one-point Gauss integration is employed for Eq. (28). By design, the employment of the strain smoothing in one-point integration passes the linear patch test and avoids the rank deficiency [44]. This approach still suffers from hourglass instability as mentioned in the introduction and is shown in our numerical investigation (cf. Figure 2). Therefore, additional stabilization will be introduced and derived in the following Sections. In addition, the pressure oscillation problem caused by the mixed formulation should be addressed with the derived stabilization method.

Remark 2.2.1 The RK approximation lacks the Kronecker delta property, and therefore, the kinematically admissible functions defined in Eq. (10) are approximated using Nitsche’s method [72] to weakly impose

the Dirichlet boundary conditions in Eq. (3). Since the focus of this study is to derive a stabilized one-point integration scheme for mixed formulation, Nitsche’s terms in the Galerkin equation are not included for clarity, as this does not affect the derivation of the proposed method.

3 Classical nodally integrated stabilization method

Here, to suppress the hourglass instability in pure one-point integration with strain smoothing, two classical approaches are employed and derived for the mixed formulation.

3.1 Subdomain smoothing stabilization

The first classical stabilization technique, as introduced in Sect. 1, is a subdomain strain smoothing method inspired by MSCNI for elasticity in the meshfree method [61, 62, 73] and in S-FEM [15, 59]. Here, subdomain strain smoothing is introduced into the domain integration for the stiffness matrix as shown below:

$$\begin{aligned}
 \mathbf{K}_{IJ}^{uu} &\approx \tilde{\mathbf{K}}_{IJ}^{uu} \\
 &= \sum_{L \in S} \left(2\mu \tilde{\mathbf{B}}_I^T(\mathbf{x}_L) \tilde{\mathbf{B}}_J(\mathbf{x}_L) W_L + \underbrace{\sum_{K \in S_L} 2\mu \left(\tilde{\mathbf{B}}_I(\mathbf{x}_L^K) - \tilde{\mathbf{B}}_I(\mathbf{x}_L) \right)^T \left(\tilde{\mathbf{B}}_I(\mathbf{x}_L^K) - \tilde{\mathbf{B}}_J(\mathbf{x}_L) \right) W_L^K}_{\text{Stabilization}} \right), \tag{29}
 \end{aligned}$$

$$\begin{aligned}
 \mathbf{K}_{IJ}^{up} &\approx \tilde{\mathbf{K}}_{IJ}^{up} = \tilde{\mathbf{K}}_{IJ}^{pu^T} \\
 &= \sum_{L \in S} \left(\tilde{\mathbf{B}}_I^T(\mathbf{x}_L) \mathbf{1} \Psi_J(\mathbf{x}_L) W_L + \underbrace{\sum_{K \in S_L} \left(\tilde{\mathbf{B}}_I(\mathbf{x}_L^K) - \tilde{\mathbf{B}}_I(\mathbf{x}_L) \right)^T \mathbf{1} \left(\Psi_J(\mathbf{x}_L^K) - \Psi_J(\mathbf{x}_L) \right) W_L^K}_{\text{Stabilization}} \right), \tag{30}
 \end{aligned}$$

$$\begin{aligned}
 \mathbf{K}_{IJ}^{pp} &\approx \tilde{\mathbf{K}}_{IJ}^{pp} \\
 &= - \sum_{L \in S} \left(\frac{1}{\lambda} \Psi_I^T(\mathbf{x}_L) \Psi_J(\mathbf{x}_L) W_L + \underbrace{\sum_{K \in S_L} \frac{1}{\lambda} \left(\Psi_I(\mathbf{x}_L^K) - \Psi_I(\mathbf{x}_L) \right)^T \left(\Psi_J(\mathbf{x}_L^K) - \Psi_J(\mathbf{x}_L) \right) W_L^K}_{\text{Stabilization}} \right). \tag{31}
 \end{aligned}$$

From Eqs. (29)–(31), the node sets S_L , \mathbf{x}_L^K , W_L^K , and $\tilde{\mathbf{B}}_I(\mathbf{x}_L^K)$ are the node sets, coordinates, quadrature weights, and the smoothed gradient matrices for the stabilization points, respectively. The stabilization points are located at the mass center of each sub-cell in each quadrature cell, as shown in Fig. 3. Different from the version for the displacement-based formulation in [61, 62, 73], the subdomain smoothing stabilization terms for the mixed formulation are applied to all coupling terms in Eqs. 29 to (31) in an analogous way. From Eqs. (29) to (31), it can be observed that the coercivity for the deviatoric and pressure part is enhanced in the discrete formulation such that low energy hourglass instability can be suppressed. However, such an approach is inefficient because of the extensive domain subdivisions. Therefore, gradient-type stabilization is proposed as shown in the following.

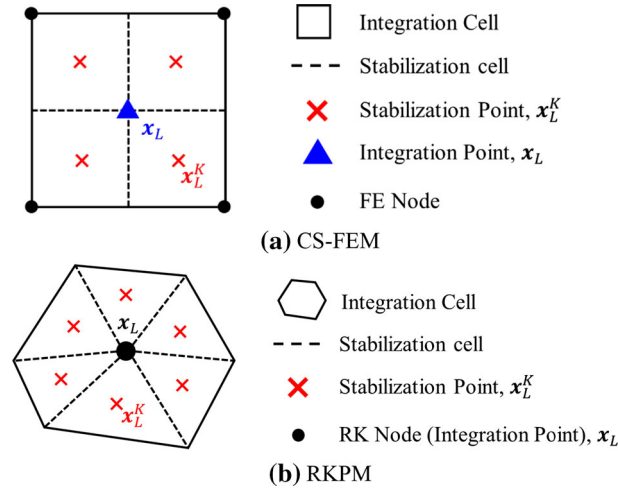


Fig. 3 Subdomain smoothing stabilization for **a** CS-FEM and **b** RKPM

3.2 Strain gradient stabilization

The second stabilization method introduced here originates from the method introduced in FEM by Liu et al. [74], RKPM by Hillman and Chen [63], and S-FEM by Yang et al. [66]. Here, this approach is extended for the mixed formulation. Following [63], a Taylor expansion is performed on the gradient for the strain and pressure as follows:

$$\boldsymbol{\varepsilon}(\mathbf{x}) \approx \boldsymbol{\varepsilon}(\mathbf{x}_L) + \sum_{i=1}^{n_d} (x_i - x_{Li}) \boldsymbol{\varepsilon}_{,i}(\mathbf{x}_L), \quad (32)$$

$$p(\mathbf{x}) \approx p(\mathbf{x}_L) + \sum_{i=1}^{n_d} (x_i - x_{Li}) p_{,i}(\mathbf{x}_L) \quad (33)$$

where n_d indicates the dimension of the problem. By substituting the gradient-expanded strain and pressure into the one-point integrated mixed formulation, the stiffness matrix below is obtained:

$$\mathbf{K}_{IJ}^{uu} \approx \tilde{\mathbf{K}}_{IJ}^{uu} + \mathbf{K}_{IJ}^{uu\nabla}, \quad (34)$$

$$\mathbf{K}_{IJ}^{up} = \mathbf{K}_{IJ}^{pu^T} \approx \tilde{\mathbf{K}}_{IJ}^{up} + \mathbf{K}_{IJ}^{up\nabla} = \tilde{\mathbf{K}}_{IJ}^{pu^T} + \mathbf{K}_{IJ}^{pu\nabla^T}, \quad (35)$$

$$\mathbf{K}_{IJ}^{pp} \approx \mathbf{K}_{IJ}^{pp} + \mathbf{K}_{IJ}^{pp\nabla} \quad (36)$$

where $\tilde{\mathbf{K}}_{IJ}^{uu}$, $\tilde{\mathbf{K}}_{IJ}^{up}$, and \mathbf{K}_{IJ}^{pp} are stiffness matrices from general strain smoothing in one-point integration as shown in Eqs. (23)–(25), and $\mathbf{K}_{IJ}^{uu\nabla}$, $\mathbf{K}_{IJ}^{up\nabla}$, and $\mathbf{K}_{IJ}^{pp\nabla}$ are stabilization terms defined, respectively, as

$$\mathbf{K}_{IJ}^{uu\nabla} = \sum_{L \in S} \sum_{i=1}^{n_d} 2\mu \mathbf{B}_{I,i}^T(\mathbf{x}_L) \mathbf{B}_{I,i}(\mathbf{x}_L) M_{iL}, \quad (37)$$

$$\mathbf{K}_{IJ}^{up\nabla} = \mathbf{K}_{IJ}^{pu\nabla^T} = \sum_{L \in S} \sum_{i=1}^{n_d} \mathbf{B}_{I,i}^T(\mathbf{x}_L) \mathbf{1} \Psi_{J,i}(\mathbf{x}_L) M_{iL}, \quad (38)$$

$$\mathbf{K}_{IJ}^{pp\nabla} = - \sum_{L \in S} \sum_{i=1}^{n_d} \frac{1}{\lambda} \Psi_{I,i}(\mathbf{x}_L) \Psi_{J,i}(\mathbf{x}_L) M_{iL} \quad (39)$$

with $\mathbf{B}_{I,i}$ the second gradient matrix defined as (for two-dimensional problem):

$$\mathbf{B}_{I,i}(\mathbf{x}_L) = \begin{bmatrix} \Psi_{I,1i}(\mathbf{x}_L) & 0 \\ 0 & \Psi_{I,2i}(\mathbf{x}_L) \\ \Psi_{I,2i}(\mathbf{x}_L) & \Psi_{I,1i}(\mathbf{x}_L) \end{bmatrix}. \quad (40)$$

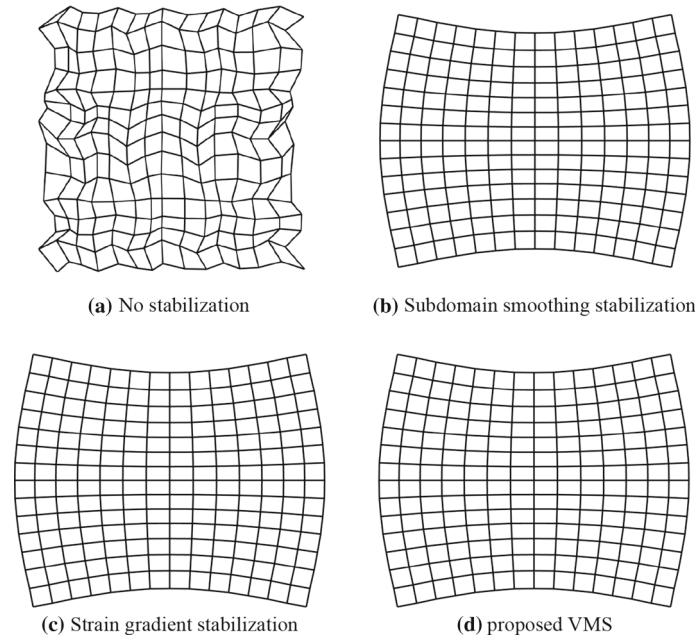


Fig. 4 Fourth eigenmodes for one-point integrated CS-FEM with and without stabilization

As general linear approximation vanishes in the computation for the higher-order direct derivative $\Psi_{I,ij}$ in Eq. (40), the strain smoothing in Eq. (28) can be adopted:

$$\tilde{\Psi}_{I,ij} = \frac{1}{V_L} \int_{\Omega_L} \Psi_{I,ij} d\Omega = \frac{1}{V_L} \int_{\partial\Omega_L} \Psi_{I,i} n_j d\Gamma. \tag{41}$$

In Eqs. (37)–(39), the term $M_{iL} = M_i(\mathbf{x}_L) = \int_{\Omega_L} (x_i - x_{Li})^2 d\Omega$ is the second moment of inertia in each integration domain. As can be seen, different from the approach shown in Sect. 3.1, the domain subdivision is avoided in the formulation and therefore is more efficient.

The use of both methods above appears to stabilize the system from the numerical results of the system eigenmodes (cf. Figs. 4, 5). However, pressure oscillations due to LBB instability remain in our numerical investigation (cf. Figs. 17, 19). As a result, the following variational multiscale method is proposed.

4 Variational multiscale stabilization method

As mentioned in Sects. 2 and 3, the current methodology in one-point integration stabilization still suffers from the LBB instability. As a result, we revisit the variational multiscale method [35] to derive an effective stabilization that is efficient and locking free. Here, a multiscale decomposition is applied to the displacement fields:

$$u_i^h(\mathbf{x}) = \bar{u}_i^h(\mathbf{x}) + \hat{u}_i^h(\mathbf{x}) \tag{42}$$

where the notations $\bar{(\cdot)}$ and $\hat{(\cdot)}$ indicate the coarse-scale and fine-scale variables, respectively. Here the term coarse and fine refers to the scale in the computational domain, not to the physical scale. Similarly, the strain can also be decoupled into two scales:

$$\varepsilon_{ij}^h(\mathbf{u}) = \varepsilon_{ij}^h(\bar{\mathbf{u}}) + \varepsilon_{ij}^h(\hat{\mathbf{u}}) = \bar{\varepsilon}_{ij}^h + \hat{\varepsilon}_{ij}^h. \tag{43}$$

In the proposed formulation, the pressure is assumed to be at a single scale:

$$p^h(\mathbf{x}) = \bar{p}^h(\mathbf{x}). \tag{44}$$

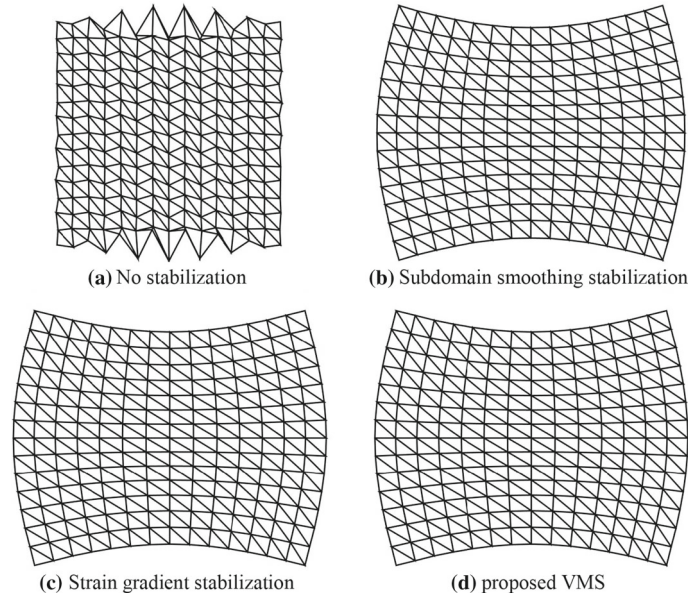


Fig. 5 Fourth eigenmodes for one-point integrated SCNI-RKPM with and without stabilization. The results are plotted on a triangular mesh for visualization purpose

It is also assumed that the Dirichlet and Neumann boundary conditions are fully controlled by the coarse-scale variables, resulting in homogeneous fine-scale boundary conditions. By introducing multiscale variables (42) into the Galerkin Eq. (10) and by decoupling the system based on the scale of the test function, we can obtain the coarse-scale problem

$$2\mu \int_{\Omega} \delta \bar{\varepsilon}_{ij}^h \varepsilon_{ij}^h d\Omega + \int_{\Omega} \delta \bar{\varepsilon}_{ii}^h \bar{p}^h d\Omega = \int_{\Omega} \delta \bar{u}_i^h b_i d\Omega + \int_{\partial\Omega_N} \delta \bar{u}_i^h t_i d\Gamma, \tag{45}$$

$$\int_{\Omega} \delta \bar{p}^h \left(\varepsilon_{ii}^h - \frac{\bar{p}^h}{\lambda} \right) d\Omega = 0 \tag{46}$$

and the fine-scale problem

$$2\mu \int_{\Omega} \delta \hat{\varepsilon}_{ij}^h \varepsilon_{ij}^h d\Omega + \int_{\Omega} \delta \hat{\varepsilon}_{ii}^h \bar{p}^h d\Omega = \int_{\Omega} \delta \hat{u}_i^h b_i d\Omega + \int_{\partial\Omega_N} \delta \hat{u}_i^h t_i d\Gamma. \tag{46}$$

Then, integration-by-parts is performed on the left hand side of Eq. (46) using coarse- and fine-scale boundary conditions, yielding Eq. (47):

$$-2\mu \int_{\Omega} \delta \hat{u}_i^h \varepsilon_{ij,j}^h d\Omega - \int_{\Omega} \delta \hat{u}_i^h \bar{p}_{,i}^h d\Omega = \int_{\Omega} \delta \hat{u}_i^h b_i d\Omega. \tag{47}$$

Decoupling the scale of the trial functions yields

$$-2\mu \int_{\Omega} \delta \hat{u}_i^h \hat{\varepsilon}_{ij,j}^h d\Omega = \int_{\Omega} \delta \hat{u}_i^h \left(2\mu \bar{\varepsilon}_{ij,j}^h + \bar{p}_{,i}^h + b_i \right) d\Omega. \tag{48}$$

From Eq. (48), it can be seen that the fine-scale solutions serve as a correction for the residual of the coarse-scale strong form equation on the right hand side of Eq. (48), such that we can approximate the fine-scale solution in the following form:

$$\hat{u}_i^h = -\tau \left(2\mu \bar{\varepsilon}_{ij,j}^h + \bar{p}_{,i}^h + b_i \right) \tag{49}$$

where τ can be approximated by a simple dimensional analysis as $\tau = c_\tau h^2/2\mu$ [24],

$$\tau = c_\tau \frac{h^2}{2\mu}, \quad (50)$$

where h is the nodal spacing and $c_\tau \in [0, 1]$ is a stabilization parameter that can be determined by the analysis of solving the local average of Green's function [39], and a value of $c_\tau = 1/12$ can be selected for linear elasticity. For different differential equations, values of $c_\tau = 0.1$ to 1.0 are often chosen [75].

Then, to introduce the fine-scale solution to the coarse-scale system, the coarse-scale Eq. (45) is reformulated using integration-by-parts for the corresponding fine-scale terms, resulting in the following equation:

$$2\mu \int_{\Omega} \delta \bar{\varepsilon}_{ij}^h \bar{\varepsilon}_{ij}^h d\Omega + \int_{\Omega} \delta \bar{\varepsilon}_{ii}^h \bar{p}^h d\Omega - \int_{\Omega} \delta \bar{\varepsilon}_{i,j}^h \hat{u}_i^h d\Omega = \int_{\Omega} \delta \bar{u}_i^h b_i d\Omega + \int_{\partial\Omega_N} \delta \bar{u}_i^h t_i d\Gamma, \quad (52)$$

$$\int_{\Omega} \delta \bar{p}^h \left(\bar{\varepsilon}_{ii}^h - \frac{\bar{p}^h}{\lambda} \right) d\Omega - \int_{\Omega} \delta \bar{p}_{,i}^h \hat{u}_i^h d\Omega = 0. \quad (53)$$

Then, by imposing the fine-scale solution, we arrive at the following formulation involving only the coarse-scale terms:

$$\begin{aligned} & 2\mu \int_{\Omega} \delta \bar{\varepsilon}_{ij}^h \bar{\varepsilon}_{ij}^h d\Omega + \int_{\Omega} \delta \bar{\varepsilon}_{ii}^h \bar{p}^h d\Omega + \int_{\Omega} 2\tau \mu \delta \bar{\varepsilon}_{ij,j}^h \bar{\varepsilon}_{ik,k}^h d\Omega + \int_{\Omega} \tau \delta \bar{\varepsilon}_{ij,j}^h \bar{p}_{,i}^h d\Omega \\ & = \int_{\Omega} \delta \bar{u}_i^h b_i d\Omega - \int_{\Omega} \tau \delta \bar{\varepsilon}_{ij,j}^h b_i d\Omega + \int_{\partial\Omega_N} \delta \bar{u}_i^h t_i d\Gamma, \end{aligned} \quad (54)$$

$$\int_{\Omega} \delta \bar{p}^h \left(\bar{\varepsilon}_{ii}^h - \frac{\bar{p}^h}{\lambda} \right) d\Omega + \int_{\Omega} 2\tau \mu \delta \bar{p}_{,i}^h \bar{\varepsilon}_{ij,j}^h d\Omega + \int_{\Omega} \tau \delta \bar{p}_{,i}^h \bar{p}_{,i}^h d\Omega = - \int_{\Omega} \tau \delta \bar{p}_{,i}^h b_i d\Omega. \quad (55)$$

Equations (54) and (55) can then be integrated by the one-point integration strain smoothing techniques in Sect. 2.2:

$$\begin{aligned} & 2\mu \int_{\Omega} \delta \hat{\bar{\varepsilon}}_{ij}^h \hat{\bar{\varepsilon}}_{ij}^h d\Omega + \int_{\Omega} \delta \hat{\bar{\varepsilon}}_{ii}^h \hat{\bar{p}}^h d\Omega + \int_{\Omega} 2\tau \mu \delta \hat{\bar{\varepsilon}}_{ij,j}^h \hat{\bar{\varepsilon}}_{ik,k}^h d\Omega + \int_{\Omega} \tau \delta \hat{\bar{\varepsilon}}_{ij,j}^h \hat{\bar{p}}_{,i}^h d\Omega \\ & = \int_{\Omega} \delta \hat{\bar{u}}_i^h b_i d\Omega - \int_{\Omega} \tau \delta \hat{\bar{\varepsilon}}_{ij,j}^h b_i d\Omega + \int_{\partial\Omega_N} \delta \hat{\bar{u}}_i^h t_i d\Gamma, \end{aligned} \quad (56)$$

$$\int_{\Omega} \delta \hat{\bar{p}}^h \left(\hat{\bar{\varepsilon}}_{ii}^h - \frac{\hat{\bar{p}}^h}{\lambda} \right) d\Omega + \int_{\Omega} 2\tau \mu \delta \hat{\bar{p}}_{,i}^h \hat{\bar{\varepsilon}}_{ij,j}^h d\Omega + \int_{\Omega} \tau \delta \hat{\bar{p}}_{,i}^h \hat{\bar{p}}_{,i}^h d\Omega = - \int_{\Omega} \tau \delta \hat{\bar{p}}_{,i}^h b_i d\Omega \quad (57)$$

where $\int_{\Omega} \hat{\cdot} d\Omega$ indicates the one-point quadrature, and $\hat{\bar{\varepsilon}}_{ij,j}^h$ and $\hat{\bar{p}}_{,i}^h$ are smoothed strain divergence and pressure gradient, respectively. To integrate the second-order gradient terms $\hat{\bar{\varepsilon}}_{ij,j}^h$ in Eqs. (56) and (57) with linear FE and RK shape functions, the smoothed divergence method in [69, 70, 75] is introduced, following the same smoothing procedure given in Eq. (22). The averaged strain divergence for the domain can be converted into a boundary integral, expressed as

$$\hat{\bar{\varepsilon}}_{ij,j}^h = \frac{1}{V_L} \int_{\Omega_L} \bar{\varepsilon}_{ij,j}^h d\Omega = \frac{1}{V_L} \int_{\partial\Omega_L} \bar{\varepsilon}_{ij}^h n_j d\Gamma = \frac{1}{2V_L} \int_{\partial\Omega_L} \bar{u}_{i,j}^h n_j + \bar{u}_{j,i}^h n_j d\Gamma, \quad (58)$$

and the strain smoothing technique can also be applied to the pressure terms:

$$\tilde{p}_{,i}^h = \frac{1}{V_L} \int_{\Omega_L} \bar{p}_{,i}^h d\Omega = \frac{1}{V_L} \int_{\partial\Omega_L} \bar{p}^h n_i d\Gamma. \quad (59)$$

Finally, using the smoothed divergence, the matrix form of Eqs. (56) and (57) can be written as

$$\begin{bmatrix} \mathbf{K}^{uu} + \hat{\mathbf{K}}^{uu} & \mathbf{K}^{up} + \hat{\mathbf{K}}^{up} \\ \mathbf{K}^{pu} + \hat{\mathbf{K}}^{pu} & \mathbf{K}^{pp} + \hat{\mathbf{K}}^{pp} \end{bmatrix} \begin{bmatrix} \mathbf{u} \\ \mathbf{p} \end{bmatrix} = \begin{bmatrix} \mathbf{F}^u + \hat{\mathbf{F}}^u \\ \hat{\mathbf{F}}^p \end{bmatrix} \quad (60)$$

where \mathbf{K} and \mathbf{F} (without $\hat{\cdot}$) are the stiffness matrices and force vectors from the SCNI scheme shown in Sect. 2, Eqs. (23)–(26), without the classical stabilization techniques mentioned in Sect. 3. $\hat{\mathbf{K}}$ and $\hat{\mathbf{F}}$ are the stiffness matrix and force vector that arise from the one-point integrated variational multiscale formulation:

$$\hat{\mathbf{K}}_{IJ}^{uu} \approx \sum_{L \in S} 2\tau\mu \left(\tilde{\nabla} \cdot \mathbf{B}_I(\mathbf{x}_L) \right)^T \left(\tilde{\nabla} \cdot \mathbf{B}_J(\mathbf{x}_L) \right) W_L, \quad (61)$$

$$\hat{\mathbf{K}}_{IJ}^{up} = \hat{\mathbf{K}}_{IJ}^{puT} \approx \sum_{L \in S} \tau \left(\tilde{\nabla} \cdot \mathbf{B}_I(\mathbf{x}_L) \right)^T \tilde{\mathbf{B}}_J^p(\mathbf{x}_L) W_L, \quad (62)$$

$$\hat{\mathbf{K}}_{IJ}^{pp} \approx \sum_{L \in S} \tau \tilde{\mathbf{B}}_I^{pT} \tilde{\mathbf{B}}_J^p W_L, \quad (63)$$

$$\hat{\mathbf{F}}_I = - \sum_{L \in S} \tau \left(\tilde{\nabla} \cdot \mathbf{B}_I(\mathbf{x}_L) \right)^T \mathbf{b} W_L, \quad (64)$$

$$\hat{\mathbf{F}}_I^p = - \sum_{L \in S} \tau \tilde{\mathbf{B}}_I^{pT} \mathbf{b} W_L \quad (65)$$

where $\tilde{\nabla} \cdot \mathbf{B}_I(\mathbf{x}_L)$ and $\tilde{\mathbf{B}}_I^p$ are the smoothed strain divergence matrix for displacement and smoothed gradient matrix for pressure, respectively. They can be expressed as

$$\tilde{\nabla} \cdot \mathbf{B}_I(\mathbf{x}_L) = \frac{1}{V_L} \int_{\partial\Omega_L} \boldsymbol{\eta} \mathbf{B}_I(\mathbf{x}) d\Gamma, \quad (66)$$

$$\tilde{\mathbf{B}}_I^p = [\tilde{\Psi}_{I,1} \quad \tilde{\Psi}_{I,2}]^T, \quad (67)$$

$$\boldsymbol{\eta} = \begin{bmatrix} n_1 & 0 \\ 0 & n_2 \\ n_2 & n_1 \end{bmatrix}^T. \quad (68)$$

Similarly, a one-point Gauss integration is used for boundary integration in Eqs. (66) and (67). The proposed variational multiscale formulation leads to a residual-based stabilization and is efficient since no domain subdivision is needed. It can also be observed that the matrices (61) and (63) serve as stabilization for deviatoric and volumetric internal energy. In addition, Eqs. (56) and (57) show that the system is symmetric and coercive; therefore, the solution will be unique and bounded.

Remark 4.1. The fine-scale solution from Eq. (48) can be solved by using a bubble function [19, 22]. However, the construction of the bubble function is complex for a meshfree discretization, and therefore, this approach is not adopted here.

Remark 4.2. For meshfree RKPM, the higher-order gradient in the stabilization term in Eq. (61) can be computed by the implicit gradient approach [76], as those in [39, 63]. Using the implicit gradient or smoothed gradient in the stabilization terms works effectively. The latter one is chosen as the implicit gradient method and is unavailable for the FE shape function.

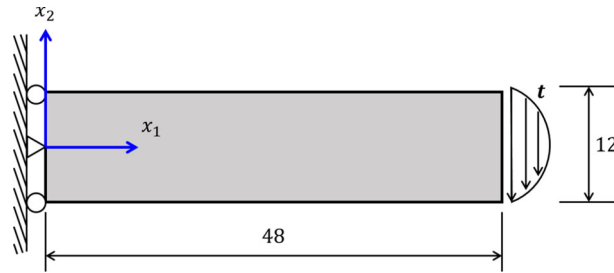


Fig. 6 Cantilever beam problem

Remark 4.3. It can be observed that the proposed one-point integrated VMS formulation exhibits some similarity to the strain gradient formulation. However, different from the NSNI formulation, the proposed method is variationally consistent, and the stabilization term for the pressure in Eq. (63) is led by the coefficient of τ (inverse of shear modulus), while the corresponding term in strain gradient formulation is led by a magnitude of $1/\lambda$.

Remark 4.4. If the terms in Eqs. (61), (62), and (64) are neglected, the proposed formulation is identical to HVM by Hughes et al. [37] and extended works (e.g., Scovazzi et al. [24]). However, this study shows that although HVM resolves the pressure oscillation issue, it is found to be unstable under one-point integration (c.f. Fig. 20 in the numerical results Section). Hence, Eqs. (61), (62), and (64) are necessary.

Remark 4.5. A single fine-scale field is employed to derive the stabilization for both displacement and pressure fields, as shown in the numerical examples (c.f. Sect. 5). Although the multiscale decomposition can also be applied to the pressure field to introduce additional stabilization, such a strategy is not adopted here. The former approach is sufficient to generate the stabilization terms (61) and (63), respectively, suppressing the instability due to low energy modes and LBB instability. The multivariable multiscale decomposition is considered in the future work of this study.

5 Numerical examples

In this Section, a series of benchmark numerical examples are analyzed to examine the performance of the proposed one-point integrated variational multiscale formulation for the material under compressible and incompressible limit. For CS-FEM, standard C^0 bilinear element (Q4) is employed. For the meshfree method, the RK approximation with linear basis and the cubic B-spline circular kernel (normalized support size 1.5) is adopted. One-point integration with the strain smoothing method is applied to all numerical schemes, unless stated otherwise, and the following three stabilization methods are adopted:

- Subdomain smoothing stabilization (Sect. 3.1)
- Strain gradient stabilization (Sect. 3.2)
- Proposed variational multiscale stabilization (Sect. 4).

5.1 Eigenmode analysis of a plate

In the first numerical example, the aim is to analyze the low-energy stability of the proposed methods by performing the eigenvalue analysis of a two-dimensional unit plate. The domain is uniformly discretized into 15 by 15 nodes (corresponding to 14 by 14 Q4 elements in CS-FEM). Young's modulus $E = 100$, and Poisson's ratio $\nu = 0.49999$. The numerical results shown in Figs. 5 and 6 indicate that the three stabilization techniques are required for CS-FEM and RKPM to avoid hourglass instability in the one-point integration method in the mixed formulation.

5.2 Cantilever beam problem

In this example, a two-dimensional cantilever beam problem under plane strain condition is considered as shown in Fig. 6. The exact displacement solution to this problem is as follows:

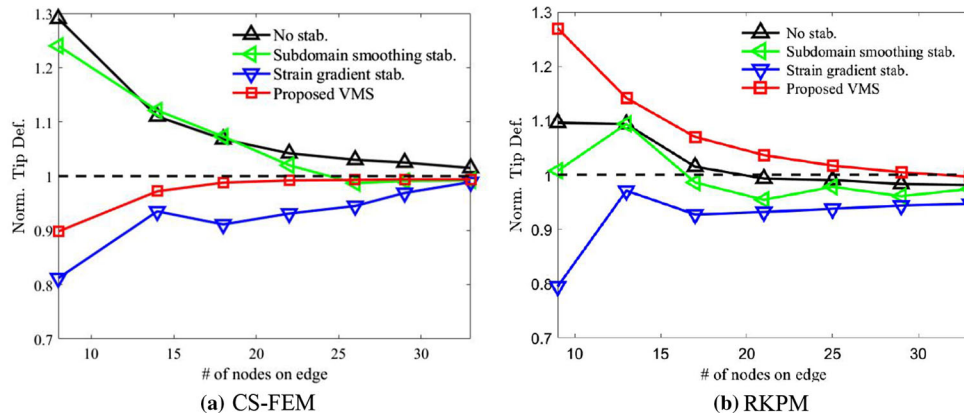


Fig. 7 Normalized tip deflection versus the edge discretization in the cantilever beam problem. The notation “stab.” is the abbreviation of “stabilization.”

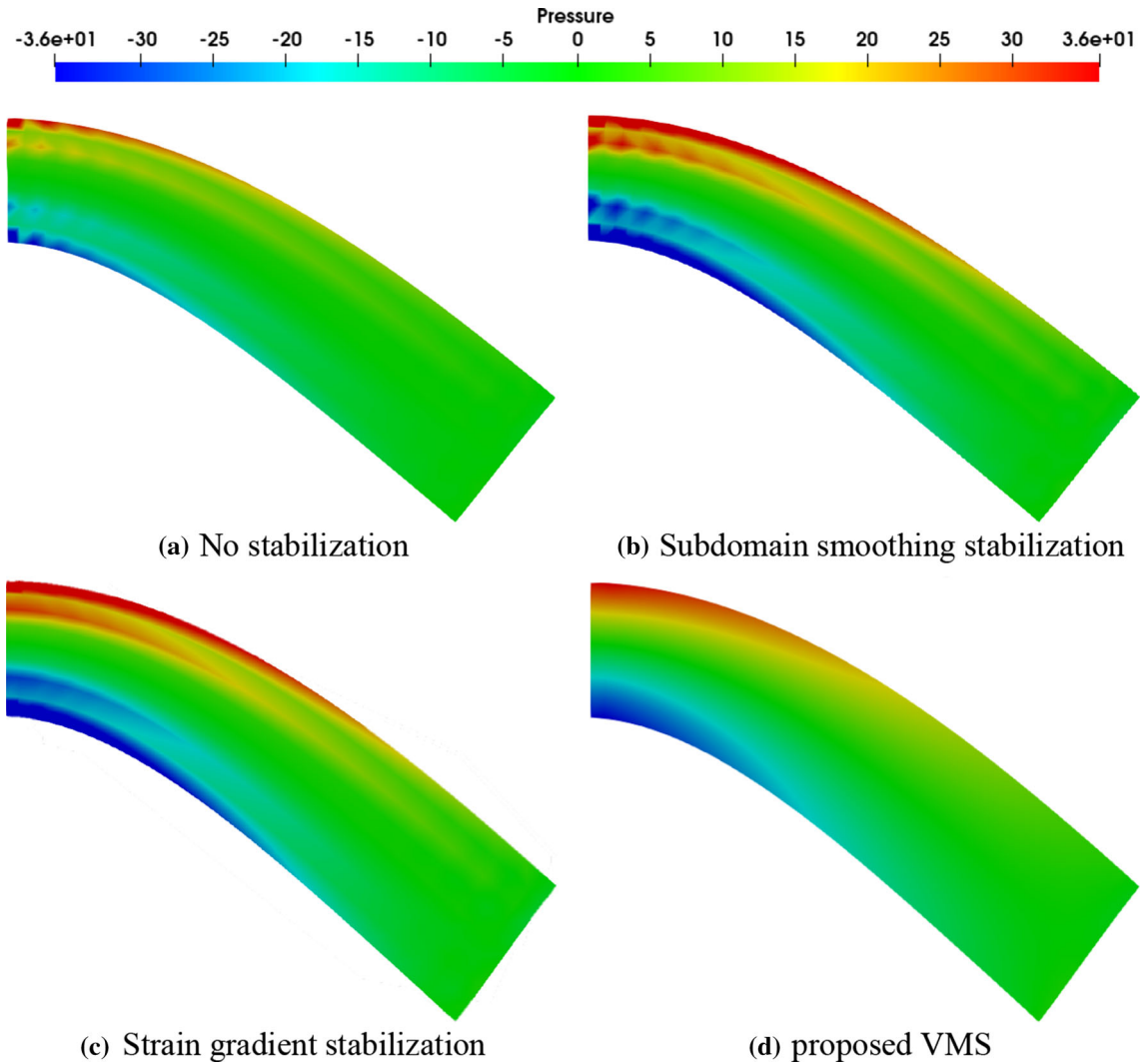


Fig. 8 Pressure distribution for CS-FEM in the cantilever beam problem

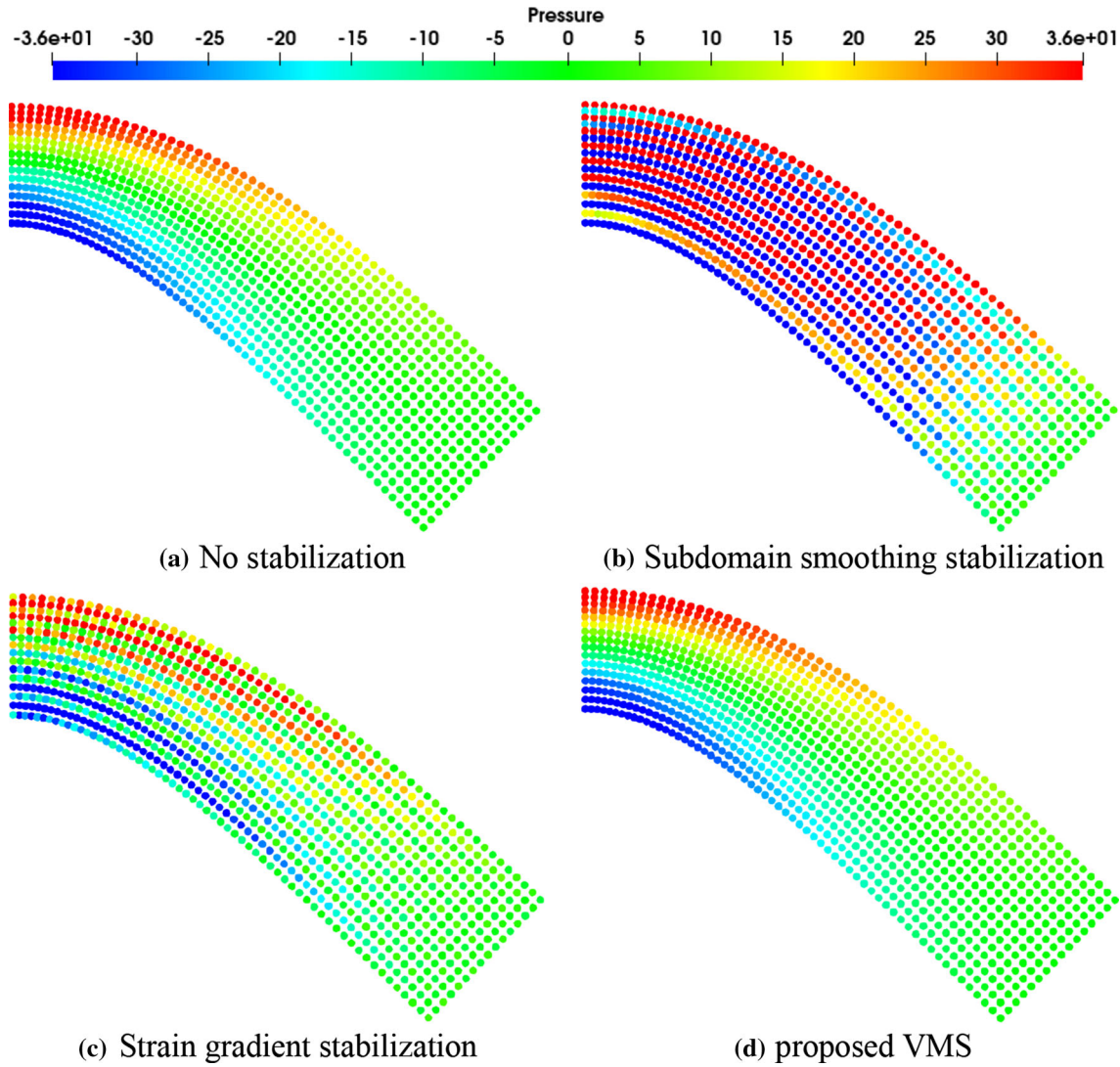


Fig. 9 Pressure distribution for RKPM in the cantilever beam problem

$$u_1^{exact} = \frac{Px_2}{6EI} \left[(6L - 3x_2)x_1 + (2 + \bar{\nu}) \left(x_2^2 - \frac{W^2}{4} \right) \right],$$

$$u_2^{exact} = \frac{-P}{6EI} \left[3\bar{\nu}x_2^2(L - x_1) + (4 + 5\bar{\nu}) \frac{W^2x_1}{4} + (3L - x_1)x_1^2 \right], \tag{69}$$

$$\bar{E} = \frac{E}{1 - \nu^2}, \bar{\nu} = \frac{\nu}{1 - \nu} \tag{70}$$

in which Young’s modulus $E = 300$, Poisson’s ratio $\nu = 0.49999$, and $P = 48$. The parameters L , W , and I are, respectively, the length, width, and second moment of inertia of the cantilever beam. The exact displacement solution is employed as the Dirichlet boundary condition on the left boundary, and Neumann boundary condition t imposed on the right boundary is computed on the basis of the exact solution. Regular discretization is employed for this problem.

In the beginning, the tip deflection normalized by the exact solution is investigated as shown in Fig. 7. It can be seen that all solutions (both with and without stabilization) converge without the locking issue, for both CS-FEM and RKPM. However, as the discretization is refined, the solution from the proposed VMS method converges faster to the exact solution compared to all other tested methods.

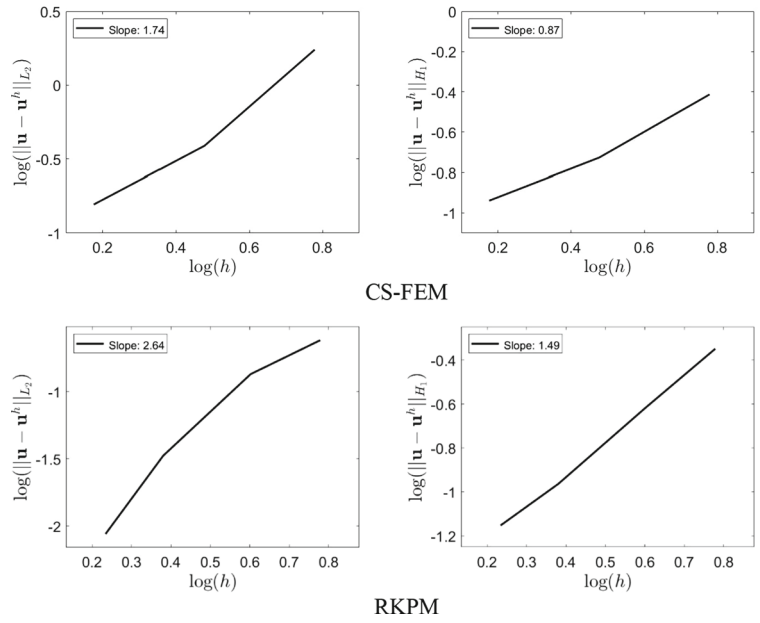


Fig. 10 Convergence study of the proposed VMS stabilized RKPM and CS-FEM in the cantilever beam problem. The value of the slope indicates the average convergence rate with given discretizations

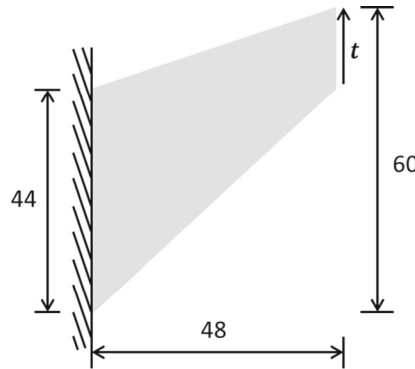


Fig. 11 Cook membrane problem: geometry and setting

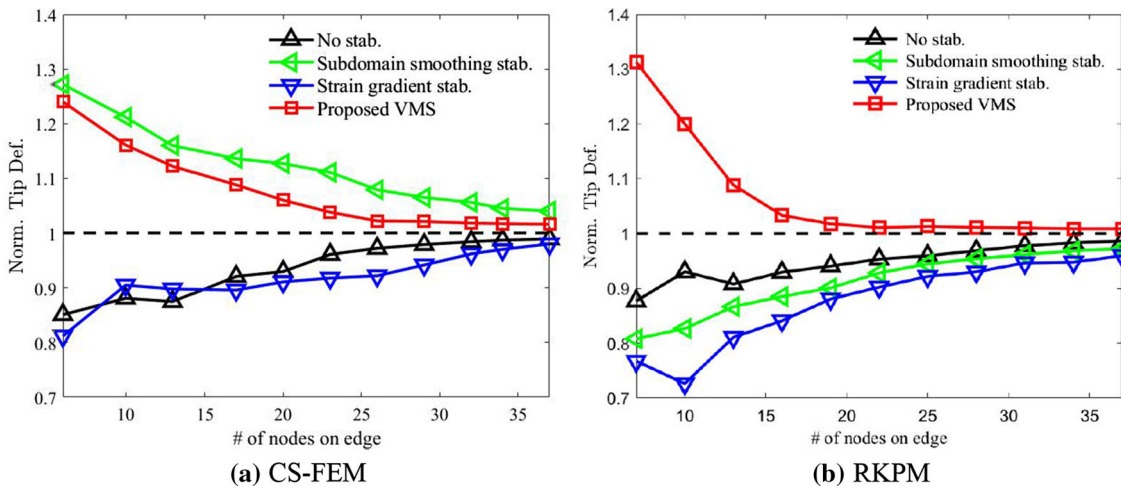


Fig. 12 Normalized tip deflection versus edge discretization in Cook's membrane problem

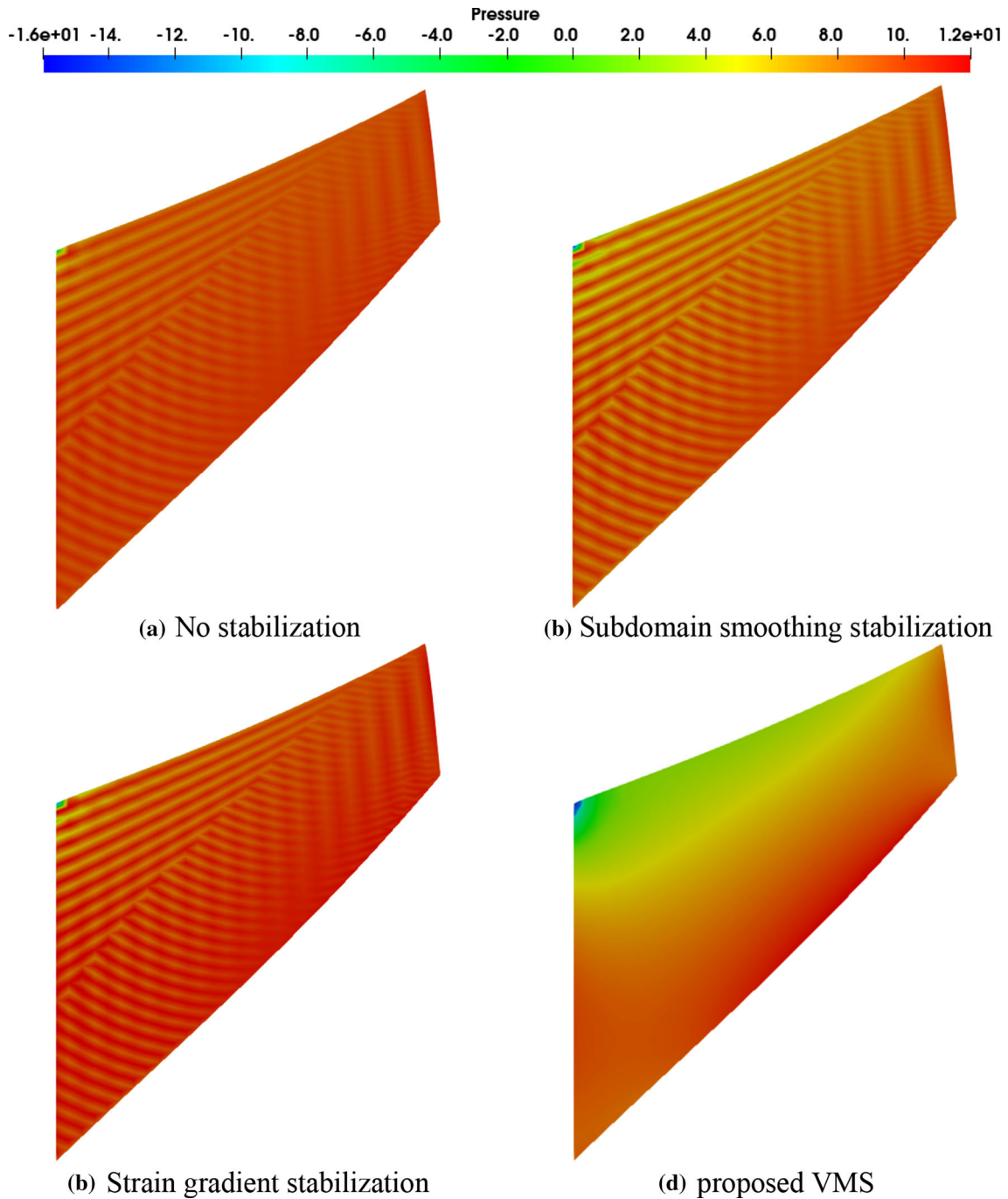


Fig. 13 Pressure distribution for CS-FEM in Cook's membrane problem

The numerical results of the pressure field from CS-FEM and RKPM for the cantilever problem can be found in Figs. 8 and 9, respectively. In CS-FEM (cf. Fig. 8), the solutions of no stabilization, subdomain smoothing stabilization, and strain gradient stabilization are all oscillatory. By contrast, in the results of RKPM (cf. Fig. 9), pure strain smoothing without any stabilization gives a stable solution, which is probably because of the higher smoothness in the RK approximation, and the solution coincidentally satisfies the LBB stability condition. However, the solution with subdomain smoothing stabilization and strain gradient stabilization is oscillatory, as the LBB stability is violated by the additional stiffness introduced by the stabilization. By contrast, the proposed method is still stable for the pressure field result. From both cases of CS-FEM and

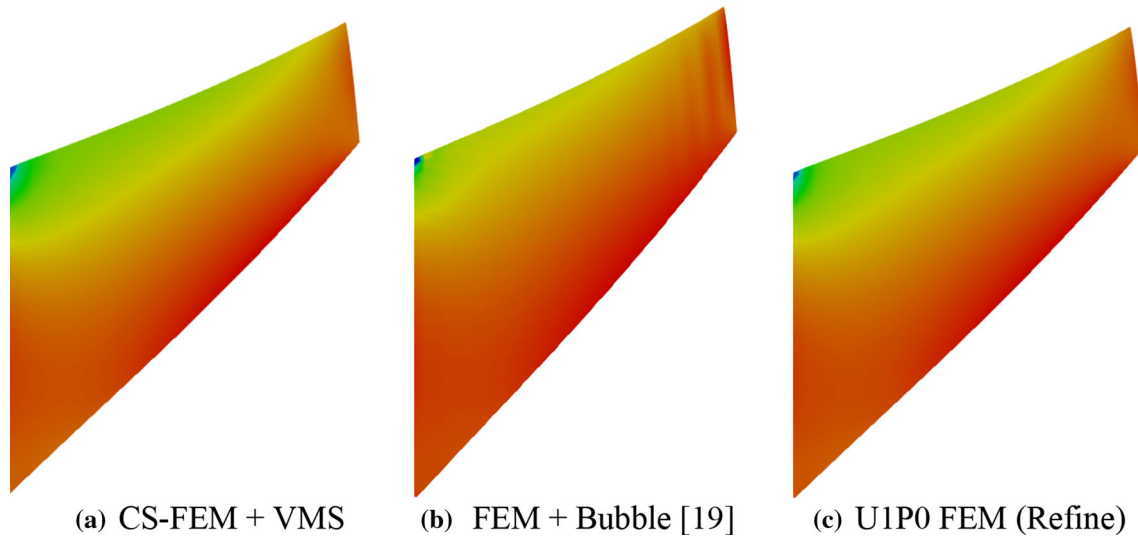


Fig. 14 Comparison of different stabilized locking-free schemes in Cook's membrane problem

RKPM, it can be concluded that the proposed VMS stabilization in a one-point integration framework works for both meshfree and mesh-based methods.

As shown in Fig. 10, the convergence study on the mesh refinement is expressed. From the numerical results, it can be easily seen that the CS-FEM and RKPM with the proposed VMS method both give optimal convergence rates in L2 and H1 without any locking issues. Specifically, the convergence rate of RKPM is better than CS-FEM, and it may be owing to the higher smoothness of the RK approximation.

5.3 Cook's membrane problem

Following the cantilever beam problem, the classical Cook's membrane problem [24] is tested. The geometry and numerical setting of the problem are shown in Fig. 11. The membrane is totally fixed on the left boundary and subjected to a shear force on the right boundary. Young's modulus and Poisson's ratio of the membrane are selected as $E = 250$ and $\nu = 0.49999$, respectively. The tip shear force is set to be $\mathbf{t} = [0, 6.25]^T$. Since there is no analytical solution, the numerical result from a refined selective deviatoric Q4 FEM is selected as the reference solution.

The convergence study of the normalized tip deflection can be found in Fig. 12. This indicates that the scheme converges as the discretization is refined, showing no locking issue. Among them, the result from the proposed VMS stabilization method converges much faster than that from the other two stabilization methods.

Similar to the previous analysis, the pressure field from CS-FEM can be observed in Fig. 13. The solutions without any stabilization, with subdomain smoothing, and strain gradient stabilization, all exhibit strong pressure oscillation. By contrast, the proposed one-point integrated variational multiscale stabilization successfully suppresses the instability.

As shown in Fig. 14, the results of the proposed method (CS-FEM + proposed VMS) are compared with those of commonly used stabilization locking-free schemes in the literature, namely the FEM + Bubble approach in [19] and the U1P0 Q4 FEM [4] with a much refined mesh. It can be seen that the results of FEM + Bubble scheme show minor oscillations near the tip. The solution of CS-FEM + proposed VMS is close to that of U1P0 FEM with a refined mesh, but with a lower computational cost owing to a coarser mesh used.

The results of RKPM in Cook's membrane problem are shown in Fig. 15. In this case, the solution without any stabilization exhibits minor instability near the left and right boundaries. However, the numerical results from the subdomain smoothing and strain gradient stabilization do not control the oscillation but aggravate the instability. By contrast, the proposed variational multiscale stabilization successfully suppresses the instability, and the solution is smooth and accurate compared to the reference solution described above.

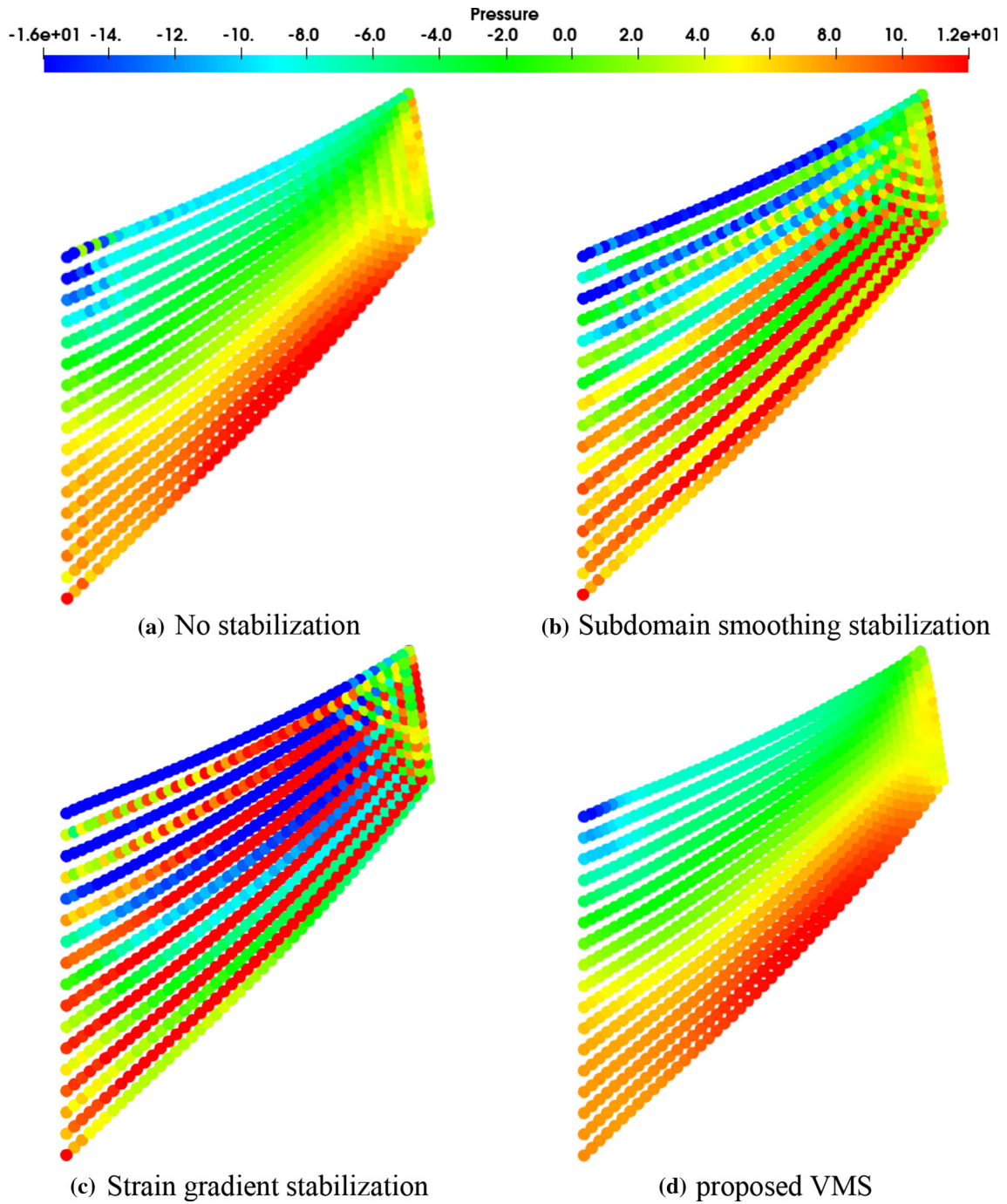


Fig. 15 Pressure distribution for RKPM in Cook's membrane problem

5.4 Punch test

A punch test mimicking the example in [14] is performed to verify the performance of the proposed scheme under a strong body-constrained condition. The numerical setting of the problem is shown in Fig. 16, where an elastic plate is totally fixed on the left, right, and bottom surfaces and is subjected to compression on the top. Young's modulus and Poisson's ratio of the plate are selected to be $E = 2 \times 10^6$ and $\nu = 0.49999$, respectively.

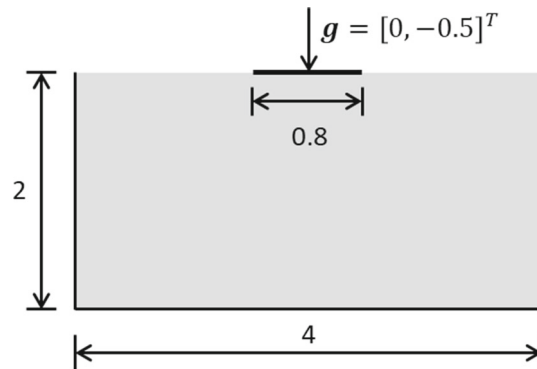


Fig. 16 Punch test: geometry and numerical setting

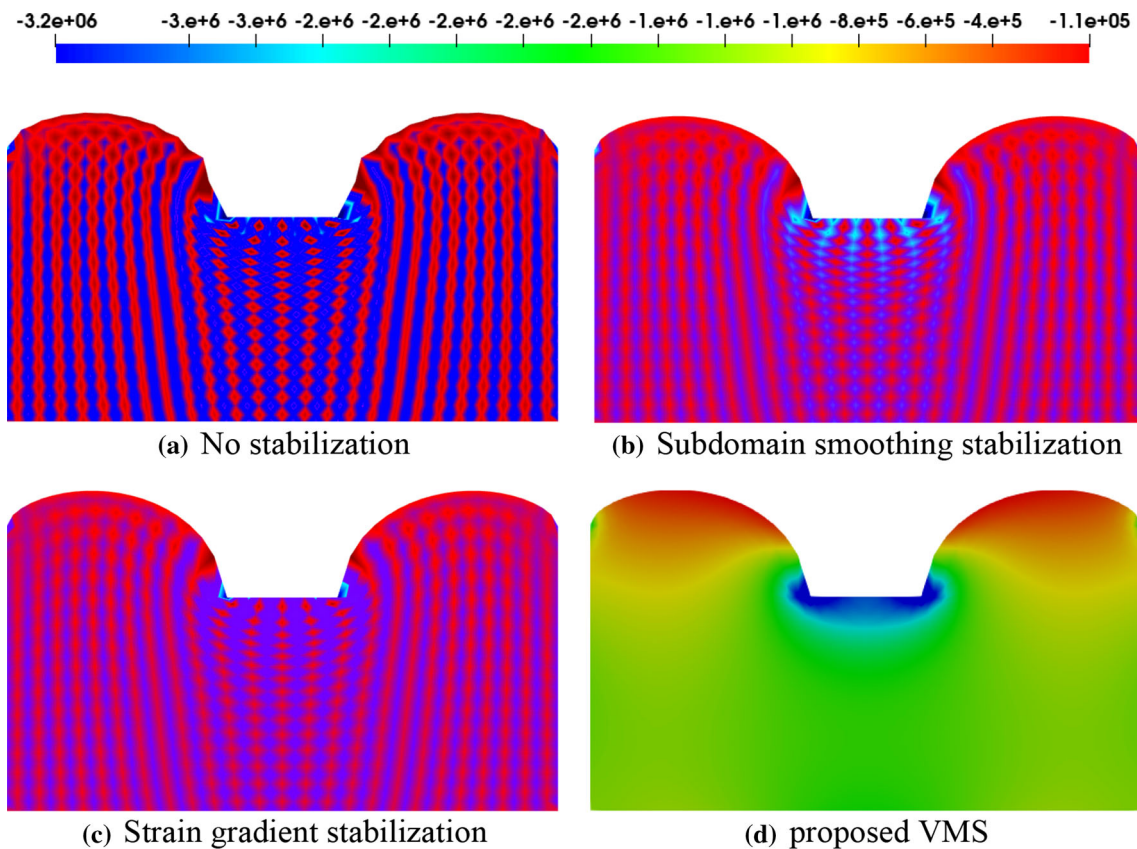


Fig. 17 Pressure distribution for CS-FEM framework in the punch test problem

Next, the numerical results of the pressure field from CS-FEM are shown in Figs. 17 and 18. Similar to the previous example, the conventional approaches in Fig. 17a–c all demonstrate strong oscillations although the plate is successfully suppressed. Hourglass instability can be found in the case of no stabilization in Fig. 17a, near the punch surfaces. The proposed VMS scheme with CS-FEM shows the most stable result.

To verify the necessity of introducing proper deviatoric and pressure stabilization as discussed in Sect. 4, the proposed scheme is compared with HVM [37], FEM + Bubble approach [19], and U1P0 Q4 FEM with a much refined mesh. As Fig. 18 shows, the results of FEM + Bubble and U1P0 Q4 FEM with refined mesh show minor instability close to the plate top surface. The solution of the proposed scheme is similar to the HVM solution, but with a smoother top surface. As the HVM scheme neglects the deviatoric stabilization when linear approximation is employed, the solution shows very small hourglass instability near the punch surface, and the severity of such instability increases further in the case of meshfree RKPM.

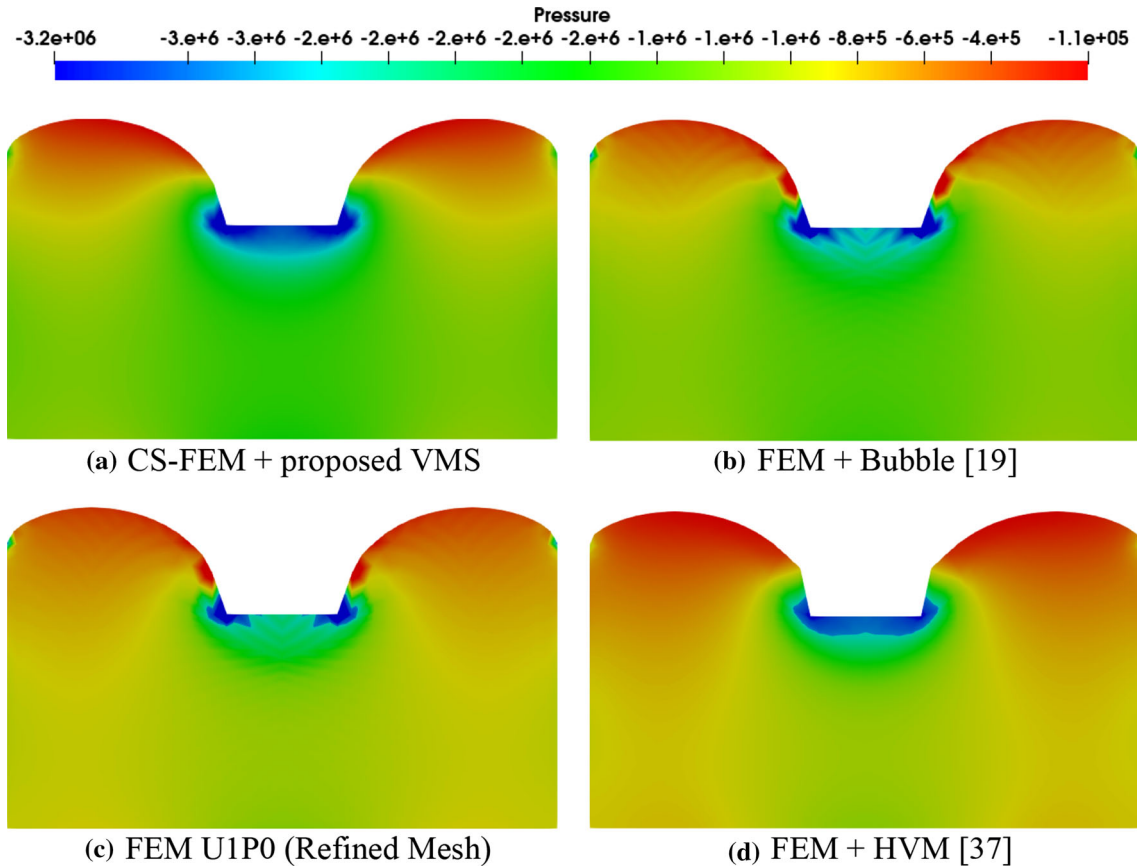


Fig. 18 Comparison of different stabilized locking-free schemes in the punch test

The pressure field from RKPM is also tested. As Fig. 19 shows, the pressure solution without any stabilization is oscillatory, and hourglass instability can be found near the punch surface. The introduction of the subdomain smoothing stabilization and strain gradient stabilization suppresses the hourglass instability such that the punch face boundary is smooth. However, the pressure fields are still oscillatory. The proposed VMS method alleviates the instability either from the hourglass modes or pressure oscillations. Continuing the investigation in Fig. 18, the results under HVM [37] and the proposed scheme are compared as shown in Fig. 20. It can be seen that the introduction of proper deviatoric stabilization in the proposed formulation, which has not been done in HVM, will ensure low energy modes and bypass the possible hourglass instability, where such instability is severer in the case of RKPM than CS-FEM.

6 Summary

In this study, a stabilized one-point integrated Galerkin mixed formulation was proposed for modeling nearly incompressible materials and applied to general meshfree and mesh-based methods, such as RKPM and FEM. In the proposed framework, the concept of SCNI was followed to employ a one-point quadrature along with strain smoothing for the mixed formulation. Then, variational multiscale stabilization was employed to address two classes of instability: (i) hourglass instability due to pure strain smoothing in the one-point quadrature rule and (ii) pressure oscillation due to the violation of the LBB condition when the equal order approximation is adopted. In this framework, the fine-scale displacement serves as a correction to the residual in the coarse-scale equations via a multiscale analysis on the variational problem. The substitution of the fine-scale solution to the coarse-scale equation naturally introduces residual-based stabilization. To retain the higher-order gradient terms in the proposed framework within the one-point quadrature rule, a smoothed divergence method was applied, which permits the employment of a lower order method such as C^0 linear FEM.

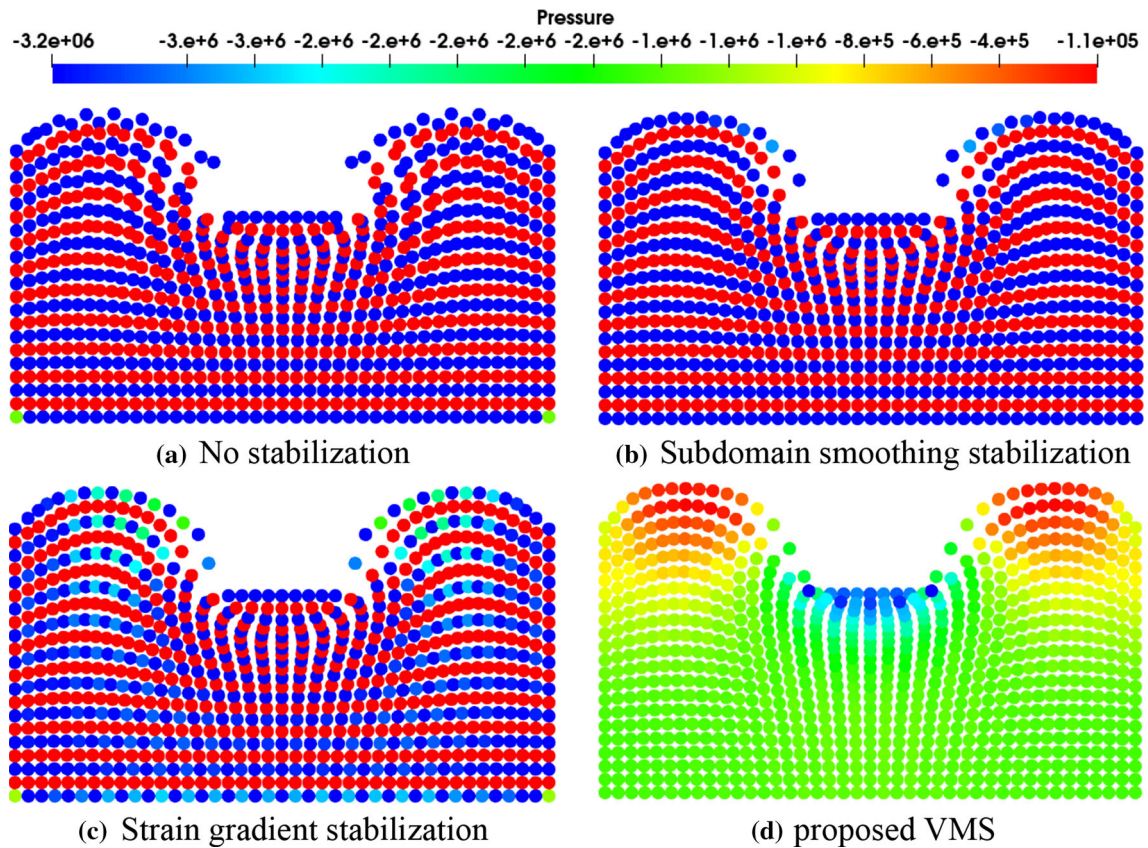


Fig. 19 Pressure distribution for RKPM in the punch test

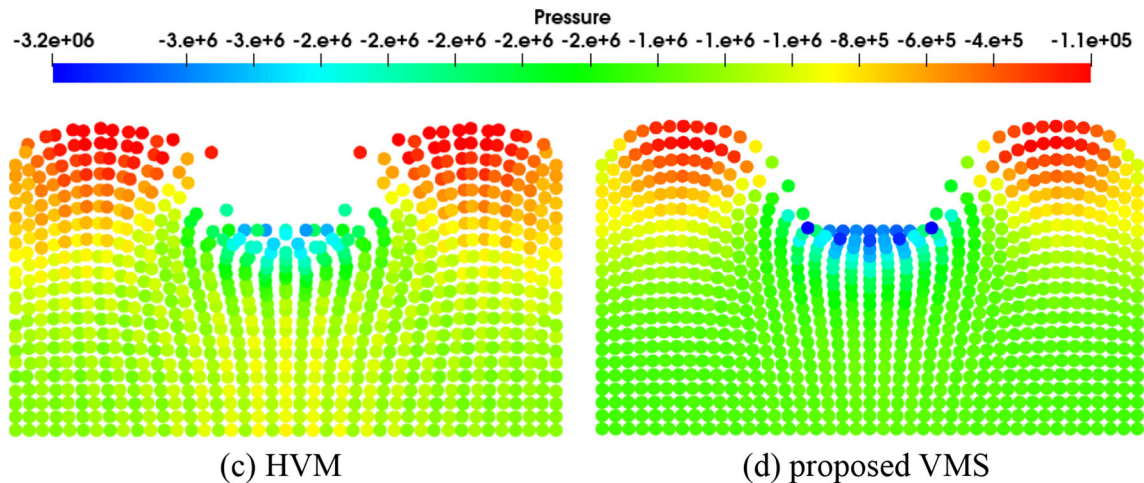


Fig. 20 Comparison between the HVM stabilization and proposed VMS stabilization in the framework of RKPM in the punch test

The effectiveness of the proposed one-point integrated variational multiscale framework was validated by solving several numerical examples and compared with two classical approaches, subdomain smoothing, and strain gradient smoothing. The proposed method exhibited better accuracy compared to the classical stabilization. In addition, although the two classical stabilization methods cured the hourglass instability, they were unstable in pressure fields because the pressure becomes more oscillatory compared to the no stabilization case. By contrast, the proposed methods suppressed the instability from the hourglass modes and

pressure oscillations due to a violation of the LBB condition. This computational framework is planned to be extended to semi-Lagrangian discretization [77] and variationally consistent integration algorithms [78] in the future, which will enable a practical framework for general numerical approximation.

Acknowledgements The support of this work by the Ministry of Science and Technology (MOST), Taiwan, under Project Contract Number 109-2222-E-007-005-MY3 to the authors is greatly acknowledged.

Declarations

Conflict of interest The corresponding author reports no conflict of interest.

Appendix: Meshfree approximation and discretization

In this study, the meshfree reproducing kernel (RK) approximation is selected as a representative meshfree method owing to its success in modeling the solid mechanical problem as discussed in Sect. 1 [16]. The RK approximation is constructed using discrete nodes [79], as shown in Fig. 21, where the domain Ω is discretized with a set of nodes $\mathbf{x}_{I=1,2,\dots}$, and \mathbf{x}_I is the position vector of node I . The RK shape function $\Psi_I(\mathbf{x})$ can be expressed as:

$$\Psi_I(\mathbf{x}) = \mathbf{H}^T(0)\mathbf{M}^{-1}(\mathbf{x})\mathbf{H}(\mathbf{x} - \mathbf{x}_I)\Phi_a(\mathbf{x} - \mathbf{x}_I) \tag{71}$$

where the basis vector $\mathbf{H}(\mathbf{x} - \mathbf{x}_I)$ is defined as

$$\mathbf{H}^T(\mathbf{x} - \mathbf{x}_I) = [1, x_1 - x_{1I}, x_2 - x_{2I}, (x_1 - x_{1I})^2, \dots, (x_2 - x_{2I})^n] \tag{72}$$

and $\mathbf{M}(\mathbf{x})$ is the so-called moment matrix:

$$\mathbf{M}(\mathbf{x}) = \sum_{I \in G_x} \mathbf{H}(\mathbf{x} - \mathbf{x}_I)\mathbf{H}^T(\mathbf{x} - \mathbf{x}_I)\Phi_a(\mathbf{x} - \mathbf{x}_I). \tag{73}$$

In RK approximation, $\Phi_a(\mathbf{x} - \mathbf{x}_I)$ is the kernel function centered at \mathbf{x}_I with the compact support size $a_I = \tilde{c}h_I$, where \tilde{c} is the normalized support size, and h_I is the nodal spacing associated with the nodal point \mathbf{x}_I . The kernel function controls the smoothness of the approximation. The following C^2 cubic B-spline kernel function is used for this study:

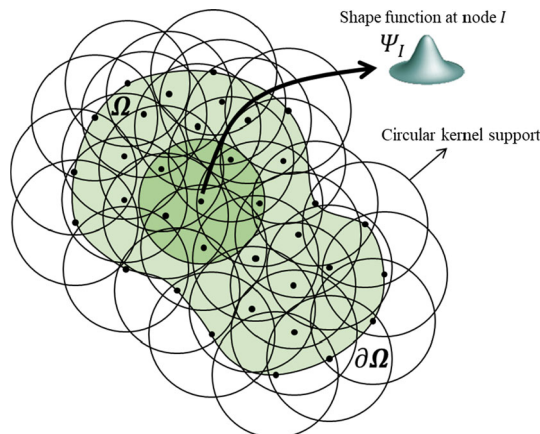


Fig. 21 RK approximation and discretization for a two-dimensional geometry (Courtesy of [65])

$$\Phi_a(\mathbf{x} - \mathbf{x}_I) = \begin{cases} 2/3 - 4z_I^2 + 4z_I^3 & \text{for } 0 \leq z_I \leq 1/2 \\ 4/3 - 4z_I + 4z_I^2 - 4/3z_I^3 & \text{for } 1/2 \leq z_I \leq 1, \\ 0 & \text{for } z_I > 1, \end{cases} \quad (74)$$

in which z_I is defined as $z_I = \frac{\mathbf{x} - \mathbf{x}_I}{a_I}$. By construction, the RK shape functions satisfy the following n^{th} order reproducing conditions in Eq. (75):

$$\sum_{I \in G_x} \Psi_I(\mathbf{x}) x_{1I}^i x_{2I}^j x_{3I}^k = x_1^i x_2^j x_3^k, \quad 0 \leq i + j + k \leq n. \quad (75)$$

References

1. Taylor, R.L., Beresford, P.J., Wilson, E.L.: A non-conforming element for stress analysis. *Int. J. Numer. Methods Eng.* **10**(6), 1211–1219 (1976)
2. Simo, J.C., Rifai, M.: A class of mixed assumed strain methods and the method of incompatible modes. *Int. J. Numer. Methods Eng.* **29**(8), 1595–1638 (1990)
3. Simo, J., Taylor, R.L., Pister, K.: Variational and projection methods for the volume constraint in finite deformation elastoplasticity. *Comput. Methods Appl. Mech. Eng.* **51**(1–3), 177–208 (1985)
4. Hughes, T.J.: *The Finite Element Method: Linear Static and Dynamic Finite Element Analysis*. Courier Corporation, North Chelmsford (2012)
5. de Souza Neto, E.A., Pires, F.A., Owen, D.: F-bar-based linear triangles and tetrahedra for finite strain analysis of nearly incompressible solids. Part I: formulation and benchmarking. *Int. J. Numer. Methods Eng.* **62**(3), 353–383 (2005)
6. Moutsanidis, G., Koester, J.J., Tupek, M.R., Chen, J.-S., Bazilevs, Y.: Treatment of near-incompressibility in meshfree and immersed-particle methods. *Comput. Part. Mech.* **7**(2), 309–327 (2020)
7. Chen, J.-S., Pan, C.: A pressure projection method for nearly incompressible rubber hyperelasticity, part i: theory. *J. Appl. Mech.* **63**(4), 862–868 (1996)
8. Chen, J.-S., Wu, C.-T., Pan, C.: A pressure projection method for nearly incompressible rubber hyperelasticity, part ii: applications. *J. Appl. Mech.* **63**(4), 869–876 (1996)
9. Chen, J.-S., Wang, H.-P., Yoon, S., You, Y.: Some recent improvements in meshfree methods for incompressible finite elasticity boundary value problems with contact. *Comput. Mech.* **25**(2), 137–156 (2000)
10. Brezzi, F., Fortin, M.: *Mixed and Hybrid Finite Element Methods*. Springer, Berlin (2012)
11. Boffi, D., Brezzi, F., Fortin, M.: *Mixed Finite Element Methods and Applications*. Springer, Berlin (2013)
12. Babuska, I.: Error-bounds for finite element method, *Numerische Mathematik. Numer. Math.* **16**(4), 322–333 (1971)
13. Ortiz, A., Puso, M., Sukumar, N.: Maximum-entropy meshfree method for compressible and near-incompressible elasticity. *Comput. Methods Appl. Mech. Eng.* **199**(25–28), 1859–1871 (2010)
14. Wu, C., Hu, W., Chen, J.-S.: A meshfree-enriched finite element method for compressible and near-incompressible elasticity. *Int. J. Numer. Methods Eng.* **90**(7), 882–914 (2012)
15. Liu, G., Dai, K., Nguyen, T.T.: A smoothed finite element method for mechanics problems. *Comput. Mech.* **39**(6), 859–877 (2007)
16. Chen, J.-S., Hillman, M., Chi, S.-W.: Meshfree methods: progress made after 20 years. *J. Eng. Mech.* **143**(4), 04017001 (2017)
17. Zeng, W., Liu, G.: Smoothed finite element methods (S-FEM): an overview and recent developments. *Arch. Comput. Methods Eng.* **25**(2), 397–435 (2018)
18. Moutsanidis, G., Li, W., Bazilevs, Y.: Reduced quadrature for FEM, IGA and meshfree methods. *Comput. Methods Appl. Mech. Eng.* **373**, 113521 (2021)
19. Masud, A., Xia, K.: A stabilized mixed finite element method for nearly incompressible elasticity. *J. Appl. Mech.* **72**(5), 711–720 (2005)
20. Nakshatrala, K., Masud, A., Hjelmstad, K.: On finite element formulations for nearly incompressible linear elasticity. *Comput. Mech.* **41**(4), 547–561 (2008)
21. Wei, H., Chen, J.-S., Hillman, M.: A stabilized nodally integrated meshfree formulation for fully coupled hydro-mechanical analysis of fluid-saturated porous media. *Comput. Fluids* **141**, 105–115 (2016)
22. Masud, A., Xia, K.: A variational multiscale method for inelasticity: application to superelasticity in shape memory alloys. *Comput. Methods Appl. Mech. Eng.* **195**(33–36), 4512–4531 (2006)
23. Masud, A., Truster, T.J.: A framework for residual-based stabilization of incompressible finite elasticity: stabilized formulations and F methods for linear triangles and tetrahedra. *Comput. Methods Appl. Mech. Eng.* **267**, 359–399 (2013)
24. Scovazzi, G., Carnes, B., Zeng, X., Rossi, S.: A simple, stable, and accurate linear tetrahedral finite element for transient, nearly, and fully incompressible solid dynamics: a dynamic variational multiscale approach. *Int. J. Numer. Methods Eng.* **106**(10), 799–839 (2016)
25. Maniatty, A.M., Liu, Y., Klaas, O., Shephard, M.S.: Higher order stabilized finite element method for hyperelastic finite deformation. *Comput. Methods Appl. Mech. Eng.* **191**(13–14), 1491–1503 (2002)
26. Wei, H., Chen, J.-S., Beckwith, F., Baek, J.: A naturally stabilized semi-Lagrangian meshfree formulation for multiphase porous media with application to landslide modeling. *J. Eng. Mech.* **146**(4), 04020012 (2020)
27. Maniatty, A.M., Liu, Y., Klaas, O., Shephard, M.S.: Stabilized finite element method for viscoplastic flow: formulation and a simple progressive solution strategy. *Comput. Methods Appl. Mech. Eng.* **190**(35–36), 4609–4625 (2001)

28. Ramesh, B., Maniatty, A.M.: Stabilized finite element formulation for elastic–plastic finite deformations. *Comput. Methods Appl. Mech. Eng.* **194**(6–8), 775–800 (2005)
29. Chiumenti, M., Valverde, Q., de Saracibar, C.A., Cervera, M.: A stabilized formulation for incompressible plasticity using linear triangles and tetrahedra. *Int. J. Plast* **20**(8–9), 1487–1504 (2004)
30. Malkus, D.S., Hughes, T.J.: Mixed finite element methods—reduced and selective integration techniques: a unification of concepts. *Comput. Methods Appl. Mech. Eng.* **15**(1), 63–81 (1978)
31. Chen, J.-S., Han, W., Wu, C., Duan, W.: On the perturbed Lagrangian formulation for nearly incompressible and incompressible hyperelasticity. *Comput. Methods Appl. Mech. Eng.* **142**(3–4), 335–351 (1997)
32. Kadapa, C., Dettmer, W., Peric, D.: Subdivision based mixed methods for isogeometric analysis of linear and nonlinear nearly incompressible materials. *Comput. Methods Appl. Mech. Eng.* **305**, 241–270 (2016)
33. Cottrell, J.A., Hughes, T.J., Bazilevs, Y.: *Isogeometric Analysis: Toward Integration of CAD and FEA*. Wiley, Hoboken (2009)
34. Schroder, J., Viebahn, N., Wriggers, P., Auricchio, F., Steeger, K.: On the stability analysis of hyperelastic boundary value problems using three-and two-field mixed finite element formulations. *Comput. Mech.* **60**(3), 479–492 (2017)
35. Hughes, T.J., Feijoo, G.R., Mazzei, L., Quincy, J.-B.: The variational multiscale method—a paradigm for computational mechanics. *Comput. Methods Appl. Mech. Eng.* **166**(1–2), 3–24 (1998)
36. Hughes, T.J., Franca, L.P.: A new finite element formulation for computational fluid dynamics: VII. The Stokes problem with various well-posed boundary conditions: symmetric formulations that converge for all velocity/pressure spaces. *Comput. Methods Appl. Mech. Eng.* **65**(1), 85–96 (1987)
37. Hughes, T.J., Franca, L.P., Balestra, M.: A new finite element formulation for computational fluid dynamics: V. Circumventing the Babuska-Brezzi condition: a stable Petrov-Galerkin formulation of the Stokes problem accommodating equal-order interpolations. *Comput. Methods Appl. Mech. Eng.* **59**(1), 85–99 (1986)
38. Franca, L.P., Hughes, T.J., Loula, A.F., Miranda, L.: A new family of stable elements for nearly incompressible elasticity based on a mixed Petrov-Galerkin finite element formulation. *Numer. Math.* **53**(1–2), 123–141 (1988)
39. Huang, T.-H., Chen, J.-S., Tupek, M.R., Beckwith, F.N., Koester, J.J., Fang, H.E.: A variational multiscale immersed meshfree method for heterogeneous materials. *Comput. Mech.* **67**(4), 1059–1097 (2021)
40. Chiumenti, M., Valverde, Q., De Saracibar, C.A., Cervera, M.: A stabilized formulation for incompressible elasticity using linear displacement and pressure interpolations. *Comput. Methods Appl. Mech. Eng.* **191**(46), 5253–5264 (2002)
41. Cervera, M., Chiumenti, M., Valverde, Q., de Saracibar, C.A.: Mixed linear/linear simplicial elements for incompressible elasticity and plasticity. *Comput. Methods Appl. Mech. Eng.* **192**(49–50), 5249–5263 (2003)
42. Codina, R.: Stabilization of incompressibility and convection through orthogonal sub-scales in finite element methods. *Comput. Methods Appl. Mech. Eng.* **190**(13–14), 1579–1599 (2000)
43. Zeng, X., Scovazzi, G., Abboud, N., Colomes, O., Rossi, S.: A dynamic variational multiscale method for viscoelasticity using linear tetrahedral elements. *Int. J. Numer. Methods Eng.* **112**(13), 1951–2003 (2017)
44. Chen, J.-S., Wu, C.-T., Yoon, S., You, Y.: A stabilized conforming nodal integration for Galerkin mesh-free methods. *Int. J. Numer. Methods Eng.* **50**(2), 435–466 (2001)
45. Chen, J.-S., Yoon, S., Wu, C.-T.: Non-linear version of stabilized conforming nodal integration for Galerkin mesh-free methods. *Int. J. Numer. Methods Eng.* **53**(12), 2587–2615 (2002)
46. Elmer, W., Chen, J., Puso, M., Taciroglu, E.: A stable, meshfree, nodal integration method for nearly incompressible solids. *Finite Elem. Anal. Des.* **51**, 81–85 (2012)
47. Wu, C., Hu, W.: Meshfree-enriched simplex elements with strain smoothing for the finite element analysis of compressible and nearly incompressible solids. *Comput. Methods Appl. Mech. Eng.* **200**(45–46), 2991–3010 (2011)
48. Liu, G., Nguyen, T., Dai, K., Lam, K.: Theoretical aspects of the smoothed finite element method (SFEM). *Int. J. Numer. Methods Eng.* **71**(8), 902–930 (2007)
49. Dai, K.-Y., Liu, G.-R., Nguyen, T.-T.: An n-sided polygonal smoothed finite element method (nSFEM) for solid mechanics. *Finite Elem. Anal. Des.* **43**(11–12), 847–860 (2007)
50. Liu, G., Nguyen-Thoi, T., Nguyen-Xuan, H., Lam, K.: A node-based smoothed finite element method (NS-FEM) for upper bound solutions to solid mechanics problems. *Comput. Struct.* **87**(1–2), 14–26 (2009)
51. Liu, G., Zhang, G.: A normed G space and weakened weak (W2) formulation of a cell-based smoothed point interpolation method. *Int. J. Comput. Methods* **6**(1), 147–179 (2009)
52. Liu, G., Zhang, G.: Edge-based smoothed point interpolation methods. *Int. J. Comput. Methods* **5**(4), 621–646 (2008)
53. Cui, X., Liu, G., Li, G., Zhang, G., Sun, G.: Analysis of elastic–plastic problems using edge-based smoothed finite element method. *Int. J. Press. Vessels Pip.* **86**(10), 711–718 (2009)
54. Zeng, W., Liu, G., Jiang, C., Dong, X., Chen, H., Bao, Y., Jiang, Y.: An effective fracture analysis method based on the virtual crack closure-integral technique implemented in CS-FEM. *Appl. Math. Model.* **40**(5–6), 3783–3800 (2016)
55. Lee, C.-K., Mihai, L.A., Hale, J.S., Kerfriden, P., Bordas, S.P.: Strain smoothing for compressible and nearly-incompressible finite elasticity. *Comput. Struct.* **182**, 540–555 (2017)
56. Jiang, C., Zhang, Z.-Q., Han, X., Liu, G.-R.: Selective smoothed finite element methods for extremely large deformation of anisotropic incompressible bio-tissues. *Int. J. Numer. Methods Eng.* **99**(8), 587–610 (2014)
57. Ong, T.H., Heaney, C.E., Lee, C.-K., Liu, G., Nguyen-Xuan, H.: On stability, convergence and accuracy of bES-FEM and bFS-FEM for nearly incompressible elasticity. *Comput. Methods Appl. Mech. Eng.* **285**, 315–345 (2015)
58. Hillman, M., Chen, J.-S., Chi, S.-W.: Stabilized and variationally consistent nodal integration for meshfree modeling of impact problems. *Comput. Part. Mech.* **1**(3), 245–256 (2014)
59. Nguyen-Xuan, H., Nguyen, H.V., Bordas, S., Rabczuk, T., Duflo, M.: A cell-based smoothed finite element method for three dimensional solid structures. *KSCE J. Civ. Eng.* **16**(7), 1230–1242 (2012)
60. Zhang, Z.-Q., Liu, G.: Solution bound and nearly exact solution to nonlinear solid mechanics problems based on the smoothed FEM concept. *Eng. Anal. Bound. Elem.* **42**, 99–114 (2014)

61. Chen, J.-S., Hu, W., Puso, M., Wu, Y., Zhang, X.: Strain smoothing for stabilization and regularization of Galerkin meshfree methods. In: Griebel, M., Schweitzer, M.A. (eds.) *Meshfree Methods for Partial Differential Equations III*, pp. 57–75. Springer, Berlin (2007)
62. Puso, M.A., Zywicki, E., Chen, J.: A new stabilized nodal integration approach. In: Griebel, M., Schweitzer, M.A. (eds.) *Meshfree Methods for Partial Differential Equations III*, pp. 207–217. Springer, Berlin (2007)
63. Hillman, M., Chen, J.-S.: An accelerated, convergent, and stable nodal integration in Galerkin meshfree methods for linear and nonlinear mechanics. *Int. J. Numer. Methods Eng.* **107**(7), 603–630 (2016)
64. Wu, C.-T., Chi, S.-W., Koishi, M., Wu, Y.: Strain gradient stabilization with dual stress points for the meshfree nodal integration method in inelastic analyses. *Int. J. Numer. Methods Eng.* **107**(1), 3–30 (2016)
65. Huang, T.-H., Wei, H., Chen, J.-S., Hillman, M.C.: RKPM2D: an open-source implementation of nodally integrated reproducing kernel particle method for solving partial differential equations. *Comput. Part. Mech.* **7**(2), 393–433 (2020)
66. Yang, H., Cui, X., Li, S., Bie, Y.: A stable node-based smoothed finite element method for metal. *Comput. Mech.* **63**(6), 1147–1164 (2019)
67. Chen, G., Qian, L., Ma, J.: A gradient stable node-based smoothed finite element method for solid mechanics problems. *Shock Vib.* **2019**, 1–24 (2019)
68. Feng, H., Cui, X., Li, G.: A stable nodal integration method with strain gradient for static and dynamic analysis of solid mechanics. *Eng. Anal. Bound. Elem.* **62**, 78–92 (2016)
69. Roth, M., Chen, J.-S., Slawson, T., Danielson, K.: Stable and flux-conserved meshfree formulation to model shocks. *Comput. Mech.* **57**(5), 773–792 (2016)
70. Huang, T.-H., Chen, J.-S., Wei, H., Roth, M.J., Sherburn, J.A., Bishop, J.E., Tupek, M.R., Fang, E.H.: A MUSCL-SCNI approach for meshfree modeling of shock waves in fluids. *Comput. Part. Mech.* **7**(2), 329–350 (2020)
71. Liu, W.K., Jun, S., Zhang, Y.F.: Reproducing kernel particle methods. *Int. J. Numer. Methods Fluids* **20**(8–9), 1081–1106 (1995)
72. Nitsche, J.: Über ein Variationsprinzip zur Lösung von Dirichlet-Problemen bei Verwendung von Teilräumen, die keinen Randbedingungen unterworfen sind. *Abh. Math. Sem. Univ. Hamburg* **36**, 9–15 (1970–1971)
73. Ruter, M.O., Chen, J.-S.: An enhanced-strain error estimator for Galerkin meshfree methods based on stabilized conforming nodal integration. *Comput. Math. Appl.* **74**(9), 2144–2171 (2017)
74. Liu, W.K., Ong, J.S.-J., Uras, R.A.: Finite element stabilization matrices—a unification approach. *Comput. Methods Appl. Mech. Eng.* **53**(1), 13–46 (1985)
75. Huang, T.-H.: A variational multiscale stabilized and locking-free meshfree formulation for Reissner-Mindlin plate problems. *Comput. Mech.* (2021). <https://doi.org/10.1007/s00466-021-02083-5>
76. Chen, J.-S., Zhang, X., Belytschko, T.: An implicit gradient model by a reproducing kernel strain regularization in strain localization problems. *Comput. Methods Appl. Mech. Eng.* **193**(27–29), 2827–2844 (2004)
77. Guan, P.-C., Chi, S.-W., Chen, J.-S., Slawson, T., Roth, M.J.: Semi-Lagrangian reproducing kernel particle method for fragment-impact problems. *Int. J. Impact Eng.* **38**(12), 1033–1047 (2011)
78. Chen, J.-S., Hillman, M., Ruter, M.: An arbitrary order variationally consistent integration for Galerkin meshfree methods. *Int. J. Numer. Methods Eng.* **95**(5), 387–418 (2013)
79. Li, S., Liu, W.K.: *Meshfree Particle Methods*. Springer, Berlin (2007)